Hydrology and
Earth System
Sciences

Open Access

Discussions

EGU

1 **Assessment of seawater intrusion using multivariate statistical, hydrochemical and**

2 **geophysical techniques in coastal aquifer, Cha-am district, Thailand**

3 Jiraporn Sae-Ju[1], Srilert Chotpantarat[1, 2, 3, 4], and Thanop Thitimakorn[1,3]

4 [1] Department of Geology, Faculty of Science, Chulalongkorn University, Bangkok 10330, Thailand

[2] Center of Excellence on Hazardous Substance Management (HSM), Chulalongkorn University,

Bangkok, Thailand.

[3] Research Program on Controls of Hazardous Contaminants in Raw Water Resources for Water Scarcity

Resilience, Center of Excellence on Hazardous Substance Management (HSM), Chulalongkorn

University, Bangkok, Thailand.

5 [4] Research Unit of Green Mining (GMM), Chulalongkorn University, Bangkok, Thailand.

[*] **Corresponding author. Tel.**: (662)2185442; **Fax.**: (662)2185464; **Email**: csrilert@gmail.com.

6

7

8

9

10

11

12

13

14

15

16

17

18   **ABSTRACT**

19   Seawater intrusion in coastal areas is one of the important environmental problems, causing negative impact

20   on groundwater resources in the future. To assess and mitigate the seawater intrusion, the affected aquifers

21   need to be characterized. By integrating geophysical investigation and multivariate statistical analysis of

22   the hydrochemical data, seawater intrusion into coastal aquifers in this area could be evaluated. The study

23   conducted 80 locations of the vertical electrical sounding (VES) survey; then selected 47 VES to create

24   four pseudo cross-section lines in a west-east direction, running perpendicular to the coast in Cha-Am

25   district, Thailand, which is negatively affected by this problem. The geophysical results were described

26   together with the hydrochemical analysis of 57 groundwater samples. The results revealed that seawater

27   intrusion occurred in the Qcl aquifer with an average depth of 50–60 meters and presented more obviously

28   near the coastal line. The resistivity value of <5 Ωm represented highly contaminated areas impacted by

29   seawater intrusion while the range between 5–10 Ωm represented moderately contaminated areas.

30   According to the hydrochemical characteristics, groundwater can be divided into three groups according to

31   the level of impact of seawater intrusion: Ca-Na-HCO$_3$ and Ca-HCO$_3$-Cl (slightly impacted), Ca-Na-HCO$_3$-

32   Cl (moderately impacted), and Na-Cl (highly impacted). The area had a low resistivity value, corresponding

33   to the high value of electrical conductivity (EC), and the hydrochemical facies was generally Na-Cl. The

34   hydrochemical facies evolution diagram (HFED) revealed that most of the samples fell close to the mixing

35   line, demonstrating mixing between seawater and fresh water and that some samples fell in the intrusion

36   phase. According to multivariate statistical analysis, the finding was in agreement with the HFED. There

37   are three main processes: seawater intrusion, natural groundwater recharge, and finally hydro-geochemical

38   interaction. Finally, the findings in this study demonstrated that the levels of seawater intrusion could be

39   classified into three zones depending on the degree of seawater intrusion. Furthermore, the northern part of

40   the study area faced seawater intrusion with a relatively higher impact than other areas, and seawater

41   laterally intruded about eight kilometers inland.

42   **Keywords:** coastal aquifer; hydrochemical facies evolution diagram; hydrogeological characteristics;

43   seawater intrusion; Thailand; vertical electrical sounding method

Hydrology and
Earth System
Sciences

Discussions

Open Access

1. INTRODUCTION

44

45   Many coastal areas in the world contain densely populations as it is an area that has food integrity

46   and important economic activities such as urban development, trade, and touristic activities. These are

47   factors that have attracted people to settle in these areas, as a result, the water demand for consumption,

48   agriculture, and industry has increased. Groundwater resources are an alternative water source. Compared

49   with surface water, the groundwater is of high quality, is barely affected by seasonal effects (i.e., constant

50   temperature), with large available quantities. For the reasons above-mentioned, groundwater has long been

51   pumped with a large quantity of water. As a result, the common phenomenon, so-called seawater intrusion,

52   has occurred in many coastal areas worldwide (Mas-Pla et al., 2014; Shi and Jiao 2014; Morgan and Werner,

53   2015).

54   In the coastal aquifer, seawater lies under fresh water since fresh water is less dense than seawater;

55   consequently, the zone of contact between fresh water and seawater is brackish water (Bear, 1999). Fresh

56   water is commonly over the top of the heavier seawater and serves to push the seawater interface seaward.

57   In contrast, when pumping fresh groundwater from coastal aquifers with a large quantity, the pressure of

58   fresh water is reduced, which in turn causes the seawater to migrate further landward. The seawater

59   intrusion problem is one of the most important environmental issues that negatively affects groundwater

60   resources significantly since groundwater salinity can lead to a reduction in fresh water availability and the

61   degradation of groundwater quality (Essink, 2001; Werner et al. 2013; Kang and Jackson 2016; Ros and

62   Zuurbier 2017). Therefore, the study of seawater intrusion into coastal aquifers is needed to identify the

63   affected zones where it should be able to prevent problems or remediate such areas efficiently.

64   The coastal study area is located at Amphoe Cha-am, Changwat Phetchabur, and was selected as it

65   is considered a densely populated area and is one of the most famous tourist areas in Thailand. Therefore,

66   the groundwater resource may become a primary water resource in the near future and is consequently

67   drawn out over the yield in the aquifer. Under this current situation, the natural equilibrium of the seawater

68   interface is directly changed, and the sea water laterally moves landward. Geophysical and hydrochemical

69   techniques have been integrated to investigate areas disturbed by seawater intrusion (McInnis et al., 2013;

70   Agoubi et al*.*, 2013; Kouzana et al*.,* 2010; Cimino et al*.*, 2008; Song et al*.,* 2006; Kazakis et al., 2016; Fadili

71   et al., 2017; Najib et al., 2017). Geophysical techniques such as the 1-D electrical resistivity survey or

72   vertical electrical sounding (VES) have been used since the electrical resistivity between fresh water and

73   seawater saturated zones show large differences (Van Dam & Meulenkamp, 1967; Sabet, 1975), therefore,

74   it is capable of identifying the contrast in terms of resistivity values between seawater and freshwater in

75   coastal aquifers. In addition, the VES technique can be enabled in large areas as it is less time-consuming

76   and has an economical cost when compared with drilling exploration methods. However, geophysical

77   survey data are not capable of identifying the clearly lateral penetration of seawater in various lithologic

78   units in a hydrogeological formation and groundwater facies or chemical constituents as the low resistivity

79   depends on various factors such as the formation materials and groundwater chemistry (Zohdy et al., 1974).

80   As a result, to fulfill the limitations of geophysics for delineating seawater intrusion areas, the integration

81   of a hydrogeological investigation (with the help of lithologic information from drill wells), chemical

82   analysis of groundwater samples, and multivariate statistical analysis were carried out. Therefore, the

83   objectives of this study were to integrate multiple techniques including multivariate statistical,

84   hydrochemical, and geophysical approaches to delineate the impact of seawater intrusion in coastal aquifers

85   in the study area and further explain the geo-hydrochemical process in the coastal aquifers.

86

87   **2. STUDY AREA**

88   The study area is located in Amphoe Cha-am, Changwat Phetchaburi, which is a part of the central

89   part of Thailand. The area covers approximately 360 square kilometers and lies between the latitudes

90   12°37.6'–12°53.845' N and longitudes 99°50.827'–99°729' E (Figure 1). The area is bounded by the

91   northern and western borders of Tha-Yang District, by the southern border of Prachuap-Khiri-Khan

92   Province, and by the eastern border of the Gulf of Thailand (Figure 1a). The area can be classified by

93   topography into two major landforms consisting of a plain interleaved mountain covers (~20% of the area)

94   and low-plain or coastal plain covers (~80% of the area). The plain interleaved mountain landform is located

95   to the west of the area, covered mainly by forest areas, while the eastern side is a low-plain or coastal plain

96   to the Gulf of Thailand, and consists of various land use types including agriculture, facilities, forests, and

97   water bodies, respectively (Land Developement Department, 2011) (Figure 1b).

98

99   *[Insert Figure 1]*

100

101   *2.1. Geological Setting*

102   The study area is located on the Shan-Thai subcontinent consisting of Carboniferous rocks to

103   Quaternary sediments as shown in Figure 2. The Permo-Carboniferous sedimentary rocks and Permian

104   limestone are the basement rocks in the area, and are found distributed to the east of the study area. In

105   addition, basement rocks intruded by Cretaceous granite that appear as a mountain range and isolate hills

106   are found in the west of the study area. The basement rocks are filled with Quaternary sediments.

107   Quaternary sediments consist of marine sediments that are coastal tide-dominate deposits, colluvial

108   sediments that accumulate around the hill foot (Department of Mineral Resources, 2014).

109

110   *[Insert Figure 2]*

111

112   *2.2. Hydrogeology*

113   The study area is underlain with unconsolidated and consolidated aquifers (see Figure 3). More

114   than 60% are underlain with the Quaternary unconsolidated aquifer that consists of a beach sand aquifer

115   (Qbs). These are common sediments in the east coastal plain and are distributed from north to south.

116   Therefore, the groundwater has accumulated in the pore space of the sand deposited in the old ridge. The

117   average depth of the aquifer is 5–8 meters with groundwater levels of approximately 1–2 meters deep. Well

118   yield is less than 2 m^3/hour. The total dissolved solid content (TDS) ranges from 500–1000 mg/L. The flood

119   plain aquifer (Qfd) is dispersed over in the upper part and is lined between Qbs and granitic aquifers (Gr).

120   The groundwater has accumulated in the pore space between the gravel and sand grains. The average depth

121   of the aquifer is 25–45 meters with groundwater levels of approximately 3–8 meters deep. Well yield is

122   between 2–10 m^3/hour, but in some areas, its range from 10–20 m^3/hour. The TDS ranged from 600–2000

123   mg/L. The colluvial sediments aquifer (Qcl) deposits near the foothill of the granite mountain are in the

124   north and south of the area. Thus, the sediments are poorly sorted, are angular to sub-angular, and the

125   groundwater has been stored in the pore spaces of the gravel, sand, quartzite fragments, granite fragments,

126   and clay deposits. The average depth of the aquifer is 30–50 meters. Well yield is relatively high at

127   approximately >50 m^3/hour. The TDS ranged widely from 300 to >1200 mg/L. The consolidated aquifers

128   are composed of 40% of the study area as described follows. The Silurian-Devonian metamorphic aquifer

129   (SDmm) was found in a small area in the lower west. The average depth of the SDmm aquifer is 30–35

130   meters with a groundwater level of approximately 3–5 meters deep. Well yield ranged from <2 m^3/hour.

131   The quality of the groundwater is generally good with a TDS <800 mg/L. The Permian-Carboniferous

132   metasedimentary aquifer (PCms) can be classified in two groups. First, in the northern part, groundwater

133   has accumulated in the fracture of mudstone and shale inter bedded with sandstone. The average depth of

134   the aquifer ranged from 50–200 meters. Well yield ranged from <2 m^3/h, but some areas can develop

135   groundwater of 5–10 m^3/h in the fracture zone. Second, in the upper eastern part of the study area,

136   groundwater has accumulated in the fracture of quartz rich sandstone interbedded with thin shale. The

137   average depth of the aquifer is 50–100 meters. Well yield ranged from 2–10 m^3/h, but some areas develop

138   groundwater of >20 m^3/h. The Permian limestone aquifer (Pc) has been found dispersing a small

139   monadnock in the north of the area. The average depth of the aquifer is 10–50 meters with a groundwater

140   level of approximately 3–5 meters. Well yield ranged between 10–20 m^3/h. The quality of groundwater is

141   good with a TDS of <500 mg/L. Finally, the Cretaceous granite aquifer (Gr) is dispersed along the large

142   mountain ranges in a north-south direction to the west of the area. The average depth of the aquifer ranged

143   from 50–150 meters with groundwater levels of 6–9 meters deep. Well yield is <2 m^3/h, but some areas can

144   develop groundwater of more than 20 m^3/h (in fracture and/or fault zones). The TDS ranged from 200–

145   1000 mg/L (Department of Groundwater Resources, 2015).

146

147   *[Insert Figure 3]*

148   **3. METHODOLOGY**

149   Seawater intrusion into coastal aquifers can be detected through several methods. In most of the

150   case studies, the electrical method has been universally recognized (George et al., 2015; Cimino et al., 2008;

151   Samouëlian et al., 2005) as the electrical conductivity (EC) of a saturated subsurface depends primarily on

152   three major factors: porosity, the connectivity of pores, and the specific conductivity of water in the pore

153   (Telford et al., 1990). The difference between the EC of the seawater saturated subsurface and freshwater

154   saturated subsurface is significant; thus, the electrical resistivity survey was well suited for evaluating the

155   relationship between freshwater and seawater in coastal areas (Sherif et al., 2006). The electrical method

156   analyzed with hydrogeological measurements can map interfaces of fresh water and seawater in coastal

157   aquifers more precisely (Zarroca et al., 2011). In this study, we used both the direct method by sampling

158   groundwater samples for hydrochemical analysis, and the indirect method by Vertical Electrical Sounding

159   (VES). Both the sampling of groundwater samples or VES investigation collected data in the dry season

160   (April to May) since seawater intrusion may occur evidently.

161   *3.1. Vertical Electrical Sounding Method*

162   One-dimensional resistivity survey, known as VES, was applied in this research. The principle of

163   VES is currently released into the ground through current electrodes A and B, then the voltage is measured

164   by potential electrodes M and N. The resistivity meter converts the voltage to the resistance value, then is

165   plotted on log-log paper in the field to check for anomalies. Eighty VES points in this research used the

166   resistivity meter (Syscal R1 Plus model, Iris) by the Schlumberger configuration (Figure 4).

167   Figure 1a shows 80 VES points which can be divided into four profiles: A-A'; B-B'; C-C'; and D-

168   D'). Four profiles were in a W-E direction oriented perpendicular to the coast line. The current electrode

169   spacing (AB) and potential electrode spacing (MN) was based on a relationship of $2(AB/2) > 5$ MN at all

170   depths (Telford et al., 1990). The current electrodes (A and B) spacing were measured in meters and varied

171   from 1 to 200 meters and the potential electrodes (P1 and P2) varied from 0.25 to 20 meters. The selected

172   current electrodes spacing were: 1, 1.5, 2, 3, 5, 7, 10, 15, 20, 25, 30, 35, 40, 45, 50, 60, 70, 80, 90, 100, 110,

173   125, 135, 150, 160, 175, 185, and 200 meters. Apparent resistivity data derived from the field was

174   interpreted using IPI2WIN software version 3.1.2c developed by Moscow State University (Bobachev,

175   2003). The data from IPI2WIN were the inversion of the apparent resistivity measurement dependent on

176   the calculation, and the calibration field curves that are compared with the theoretical curves of the program.

177   The results of the VES survey method were the resistivity of the soil and rock layers vertically. The shape

178   and slope of the VES data on the graph represents changes of the layer that had different resistivity (Telford

179   et al., 1990). Therefore, the correct interpretation of VES required the use of information regarding the local

180   geology and drilling information of the groundwater wells.

181

182   *[Insert Figure 4]*

183

184   *3.2. Chemical Analysis of Groundwater*

185   A total of 57 groundwater samples were collected in the study area. Prior to sampling, the

186   groundwater must be pumped out for 5–10 minutes to represent the groundwater in the aquifer. Samples

187   were necessary to measure physical and chemical parameters such as pH, electrical conductivity (EC),

188   groundwater, and total dissolved solids (TDS) in the field by using portable meters. Samples for the analysis

189   of cations and anions were collected in two bottles of 500 mL Poly-Ethylene (1 bottle with nitric acid

190   (HNO_3) added to maintain the acidity of the water and the other with no nitric acid to be used for anion

191   analysis. Samples were kept at 4 °C to reduce the process of microorganisms and reduce the speed of

192   physical and chemical processes. The groundwater analysis was divided into two parts: anion analysis and

193   cation analysis. Chemical analysis was carried out for a group of cations (Ca^{2+}, Mg^{2+}, Na^+, K^+, and Fe^{2+})

194   analyzed by the Absorption Spectrometry Method (AAS), whereas the group of anions (Cl^-, Br^-, NO_3^{2-}, and

195   SO_4^2) were analyzed using the Ion Chromatographic Method (IC) and CO_3^{2-}, HCO_3^- were analyzed by the

196   volumetric titration method. The results of the chemical analysis can be analyzed by the piper diagram and

197   hydrochemical facies evolution (HFE) diagrams to classify the types of water that seawater intrusion can

198   be indicated by an increase in TDS and the major ions of seawater.

Hydrology and
Earth System
Sciences
Discussions

199   Furthermore, correlation analysis and principal component analysis (PCA) were used to clearly

200   acquire the relationship among the hydrogeochemical parameters measured in the groundwater samples,

201   which enabled the identification of the hydro-geochemical processes occurring in the groundwater system.

202   In this study, the multivariate statistical technique were carried out using the SPSS software, version 22.

203   Ten hydrochemical parameters (K, Na, Fe, Ca, Mg, F, Cl, Br, SO_4, and HCO_3) as well as pH, and electrical

204   conductivity (EC) in the groundwater samples were carried out using correlation analysis and PCA. These

205   two techniques are a statistical technique to group and establish the relationship between a group of

206   groundwater samples based on hydrochemical characteristics (Abderamane et al., 2012).

207

208   **4. RESULTS AND DISCUSSION**

209   *4.1. Vertical Electrical Sounding*

210   Figure 1a shows 80 VES points. All 80 of the VES data showed the H type curve (Telford et al.,

211   1990) (Figure 5a). This implied that there were three layers in the subsurface that consisted of resistivity

212   with $\rho_1 > \rho_2 < \rho_3$ (ρ_1 = resistivity of upper layer, ρ_2 = resistivity intermediate layer ,and ρ_3 = resistivity

213   bottom layer) and were consistent with the characteristics of geology and hydrogeology of study area. The

214   top layers represented the unsaturated sediments, the middle layer was the saturated sediments, and the

215   bottom layer was interpreted as bed rock (Figure 5b).

216   *[Insert Figure 5]*

217   Figure 5b shows the results of the interpretation of VES St25 where apparent resistivity is the black

218   line and the master curve is the red line. It was found that at the St 25 location, it could be divided into four

219   layers (blue line). The top layer had a resistivity of 9.38 Ωm with a thickness of 3.11 m and a depth of 3.11

220   m. The second layer had a resistivity of 2.02 Ωm, thickness of 11.3 m, and depth of 14.4 m. The third layer

221   had a resistivity of 1.49 Ωm, thickness of 60.1 m, and a 74.5 m depth. The bottom layer was the bedrock

222   layer with a resistivity of 757 Ωm. The RMS error was 2.46%. After the layers were interpreted for all

223   points, then pseudo cross-sections for the four lines were generated.

224   The pseudo cross-sections (A-A', B-B', C-C', and D-D') were generated from 1D VES data that

225   selected 47 VES points from this study and 9 VES points from the Department of Groundwater Resources

226   (DGR) database. All cross-section lines were created from west to east that was perpendicular to the coast

227   line (Figure 1a).

228   The pseudo cross-section A-A' (Figure 6a) had 14 VES that consisted of St1, St2, St3, 42–28, St4,

229   F5, 42–29, St5, St6, F6, St7, St8, St9, and St10. This line was located at the lower part of the study area

230   and the total length was approximately 6750 m. It was found that the surface layer (0–10 m) had resistivity

231   ranging from 10–1000 Ωm. It was interpreted as an unsaturated zone of the Qfd aquifer. At the western side

232   of the profile, very high resistivity (400–1000 Ωm) was observed. This is due to the granite batholith that

233   intrudes in the base rock, as a granite outcrop was found near the St8. In the eastern side, at a depth of 130–

234   200 m, the layer that had a resistivity of 50–100 Ωm was the bedrock layer. The top of this side showed

235   resistivity values between 3–40 Ωm, and represents sediment saturated with water, especially near the

236   coastal line where there was a very low resistivity zone (<5 Ωm). This may represent the influence of

237   seawater intrusion that intrudes inland about one kilometer from the coast line.

238   The pseudo cross-section B-B' (Figure 6b) consisted of 16 VES points (St11, St12, St13, St14,

239   St15, St16, St17, St18, St19, St71, St20, St21, St22, St23, 42–126, and 42–125) and started from east to

240   west. This line was close to the A-A' profile and total distance was approximately 8450 m. It was found

241   that the surface layer (0–10 m) had resistivity anomalies between 50–400 Ωm. This represents the

242   unsaturated zone of the Qfd aquifer. The next layer showed resistivity values ranging from 2–20 Ωm. This

243   was interpreted as a sediment layer saturated with water. Near the coast line, there was a low resistivity

244   zone (<5 Ωm) that extended approximately two kilometers inland, which may represent the influence of

245   seawater intrusion. At the west side of the profile at a depth 20–200 m, there was a zone of resistivity

246   ranging from 60–250 Ωm that represented the bedrock layer.

247   The pseudo cross-section C-C' (Figure 6c) consisted of 12 VES as follows: St24, St25, St26, St27,

248   St28, St29, St30, St31, 41–205, St32, 41–191, and St33 from the east to west direction. This profile was

249   between the B-B' and D-D' profiles. The total distance of this line was approximately 7975 m. The surface

250   (0–10 m) layer had a resistivity range from 6–700 Ωm, which represented the unsaturated zone of Qfd

251   aquifer. The next layer showed resistivity values between 2–20 Ωm and represents the sediment layer

252   saturated with water, and there was a low resistivity zone (<5 Ωm) near the coast line where it extended

253   inland approximately 3.2 kilometers, representing the influence of seawater intrusion. Furthermore, the

254   western side of the profile at a depth 40–200 meters showed resistivity values between 60–200 Ωm,

255   representing the bedrock layer.

256   The pseudo cross-section D-D' (Figure 6d) consisted of 14 VES as follows: St34, St35, St36, St37,

257   St39, St41, St42, St43, St44, 41–174, 41–173, St45, St46, and St47 from an east to west direction. This

258   profile was on the northern part of the study area and the total length was approximately 14,300 m. It was

259   found that the surface (0–10 m) layer had resistivity in a range from 1.5–400 Ωm, representing the

260   unsaturated zone of the Qfd aquifer. In this profile, there were low resistivity anomalies (<5 Ωm) near the

261   surface at St7, possibly caused by the waste water from community areas. The next layer showed resistivity

262   values in a range from 1.5–20 Ωm, representing the sediment layer saturated with water. Near the coast

263   line, the low resistivity zone (<5 Ωm) extended far from the coast inland approximately four kilometers,

264   representing the influence of seawater intrusion. In the west side of the profile, the bedrock was found with

265   resistivity values of 40–100 Ωm at a depth between 90–200 meters.

266   Since soil or rock layers with low resistivity may be caused by many reasons including the clay

267   content or salt water in hydrogeologic formations, this research compared the lithologic data with the VES

268   data survey and found that the low resistivity at the area near the coast line may have been caused by the

269   seawater. Figure 7 shows the resistivity values compared with the litho-log of lines D-D'. The left side

270   shows the lithological data of well no. Q168 versus the VES of St47 that represents a position located far

271   from the coast, and the right side shows the lithological data of well no. PW7962 versus the VES of St34

272   that represents a position located near the coast. It was found that the low resistivity (<5 Ωm) at VES St34

273   corresponded to a gravelly clay layer, but at VES St47, the layer with components of clay or clayey gravel

274   showed a resistivity of only 10–20 Ωm. From the comparison, it can be concluded that although the layer

275   had a clay component, the resistivity value was not very low (<5 Ωm). As a result, the area that showed

276   very low resistivity may have been influenced by seawater intrusion. This is consistent with previous studies

277   (Ravindran, 2013; Kaya et al., 2015; Gopinath and Srinivasamoorthy, 2015) who concluded that the areas

278   with low resistivity (<5 Ωm.) were influenced by seawater intrusion.

279

280   *[Insert Figure 6]*

281   *[Insert Figure 7]*

282

283   *4.2. Geoelectrical Section*

284   When the pseudo cross-sections of the four profiles were analyzed with borehole log and electric

285   log data, the comparison of these two data was established as shown in Figure 8. The four geo-electrical

286   cross-sections clearly showed the boundaries of each aquifer. The top layer was the Qfd aquifer consisting

287   of well sorted sand with high sphericity of approximately 0–20 m thick. The next layer was the Qcl aquifer,

288   which consisted of clayey gravel (poorly sorted and angular to sub-angular) interbedded with sand in some

289   areas. The average thickness was approximately 50–60 m, but it gradually increased by 100 meters in the

290   area near the coast line. The next layer underneath the Qcl aquifer was the PCms aquifer, consisting of

291   greenish gray sandstone and shale with an average depth between 50–200 meters. In the A-A' and B-B'

292   profiles, which were located in the lower part of the study area, the PCms aquifer was not found, whereas

293   granite (Gr) aquifers could be found in all profiles. In the D-D' profile, the Pr aquifer was located in the

294   central part of profile. It lay on top of the PCms aquifer at an approximate depth of 50–60 m. Since this

295   area had a limited number of borehole log data, the interpretation to create a cross-section in some areas

296   was required as shown in the dashed line in the cross-section.

297

298   *[Insert Figure 8]*

299

300   *4.3. Apparent Resistivity Map*

Hydrology and
Earth System
Sciences
Discussions

Open Access

EGU

301   Figure 9 shows the apparent resistivity map established from the apparent resistivity of VES for

302   comparison of the resistivity of various depths. In this study, the apparent resistivity values for AB/2 = 5,

303   10, 30, 50, 70, 100, 150, and 200 meters were selected to create an apparent resistivity map by using the

304   ArcGIS9.3 program. The dark blue color on the map represents low resistivity and the red color represents

305   high resistivity, respectively. Figure 9 shows that all depths showed the location of low apparent resistivity

306   (<5 Ωm) in the same place. This was located on the east side of the study area which covered Tumbon Tha-

307   Yang, Nong-Sa-La, Bang-Kao, and some parts of Tambon Cha-Am. The maps of AB/2 = 5 and 10 meters

308   (Figures 9a and 9b) showed low apparent resistivity distributed in a sporadic pattern. This was found in a

309   wide area in the maps of AB/2 = 30, 50, and 70 m and was decreased in maps of AB/2 = 100, 150, and 200

310   m (Figure 9). The area with the highest apparent resistivity (>1000 Ωm) was located on the western side of

311   the study area covering most areas of Tumbon Khao Yai and Sam Pra Ya, corresponding to the bedrock in

312   the area. The map of AB/2 = 70 meters (Figure 9c) had the widest dark blue (<5 Ωm) area, which

313   corresponded to the depth of 50 m from the ground surface when compared to the cross-section;

314   consequently, it was found that this depth was located in the Qcl aquifer. As a result, it can be concluded

315   that the Qcl aquifer has been highly influenced by seawater intrusion.

316

317   *[Insert Figure 9]*

318

319   *4.4. Groundwater Chemistry*

320   The hydrochemical analysis of 58 groundwater samples is shown in Table 1. The total dissolved

321   solids (TDS) ranged from 195–3580 mg/L. The electrical conductivity (EC) of the groundwater samples

322   ranged from 292–5360 mS/cm. Figure 8 shows the hydrochemical facies classification of the groundwater

323   samples with the chemical result plotted on a piper diagram (Galloway & Kaiser, 1980) by the Groundwater

324   Chart Program from United States Geological Survey (USGS). The reliability of the results of the

325   hydrochemical analysis determined the charge balance of cation and anion (%Δ, which in this study was

326   acceptable at %Δ <10 (ALS Environmental). From Table 1, it was found that 42 samples were acceptable

327 (%Δ <10) and could be further used for discussion and interpretation while the unreliable results of 16

328 samples may have resulted from the process of groundwater collection and preservation, as well as the

329 dilution of the concentration of samples.

330 Figure 8 presents the piper diagram that shows the hydrochemical facies classification of 42

331 samples. The piper diagram can be divided into five facies as follows: the Ca-Na-HCO$_3$, Ca-HCO$_3$-Cl, Ca-

332 Na- HCO$_3$-Cl, Ca-Na-Cl, and Na-Cl facies represent fresh water and were found in W5, which was opened

333 as a well screen to the Gr aquifer. This groundwater facie is younger and is weakly acidic, which is generally

334 found in high terrain or recharge areas (Appelo and Postma, 2005). The Ca-HCO$_3$-Cl facie was found in

335 W19 and W20 that were opened as a well screen to the Gr aquifer. This facie was in water-bearing

336 permeable rocks given that when groundwater moves through the rock formation, the ion exchange process

337 takes place (Appelo & Postma, 2005). The quality of the water in this facie is fresh water. The Ca-Na-

338 HCO$_3$-Cl facie was found in 21 wells, which opened the well screen in four aquifers as follows: Gr aquifer

339 (eight wells), PCms aquifer (nine wells), Pr aquifer (one well, namely, W52), and Qcl (three wells). This

340 facie presents a complex chemical pattern since the water was influenced by many factors. This may have

341 resulted from the mixing of fresh water with seawater (Appelo and Postma, 2005). The Ca-Na-Cl facie was

342 found in W53 that was opened as a well screen to the Pr aquifer, while three wells (W24, W25, and W34)

343 were opened as a well screen to the Qcl aquifer, and two wells (W22 and W23) were opened as a well

344 screen to both the Qcl and PCms aquifers. The groundwater facies may have been changed due to the

345 influence of seawater intrusion by the ion exchange process (Appelo and Postma, 2005). The Na-Cl facie

346 was found in 10 wells that were opened as a well screen to the Qcl aquifer. The groundwater facie indicated

347 that these wells were influenced by seawater intrusion, and the quality of the water was saline water.

348

349 *[Insert Table 1]*

350

351 According to the piper diagram by Galloway and Kaiser (1980), the groundwater facie can be

352 classified into five facies, which correspond to the influence of seawater intrusion, and not only depend on

353   the distance from the coast, but also on the depth of the well or the screen level of the well. Most of the

354   groundwater samples in the Qcl aquifer were relatively influenced by seawater intrusion. In general, an

355   average depth of the Qcl aquifer ranged from 20–50 m and the thickness was typically higher than 100

356   meters approaching the coast line. The Na-Cl facies (approximately ~48%) and the Ca-Na-Cl facies

357   (approximately ~19%) were mainly found in the Qcl aquifer. The remaining approximate 20% of the

358   groundwater wells represented Ca-Na-HCO$_3$-Cl. According to the geochemical facies, the average

359   composition of cations (in meq/L) in the Qcl aquifer was in the following order: Na >> Ca > Mg~K.

360   Furthermore, the composition of anions (in meq/L) in the aquifer was in the descending order: Cl >> HCO$_3$

361   > CO$_3$ > SO$_4$. Therefore, their hydrochemical composition could be addressed as seawater intrusion in this

362   aquifer (Ahmed et al., 2017). The groundwater facies in the PCms and Gr aquifers, which opened a well

363   screen in the high weathering zone (underneath Qcl aquifer) at a depth of 40–60 meters was composed of

364   the Ca-Na-HCO$_3$-Cl facies, suggesting that the groundwater was moderately affected by seawater intrusion.

365   Moreover, the groundwater facies in the PCms and Gr aquifers (where a well screen opened at a depth of

366   60–80 meters) were the Ca-HCO$_3$-Cl and Ca-Na-HCO3 facies, suggesting that the groundwater was slightly

367   affected by seawater intrusion due to the mixing of recharge rainwater.

368   The relationship between the depth variation with the Cl and Na concentrations in each aquifer is

369   shown in the Supplementary Information (Figure SI.1). The chloride concentration was mostly found in

370   relatively high concentrations in the Qcl aquifer, especially in shallow to moderate depths (approx. 15 to

371   70 m depth). However, this relationship of salinity with depth was not well correlated in the Pcms and Gr

372   aquifers, implying that the groundwater in these aquifers were not highly impacted by seawater intrusion.

373   The red line on the piper diagram (Figure 10) is the line that shows the hydrochemical evolution of

374   the groundwater facies by the cation exchange reaction (Appelo & Postma, 2005). This line resulted from

375   two points plotted between the composition of seawater (blue point) and fresh water (red point) on the piper

376   diagram. By using this line, the hydrochemical results of the groundwater samples fall in the zone between

377   the blue and red points, representing mixed water occurring between the fresh water and seawater. The

378   groundwater facies close to the blue point were Na-Cl facies and Ca-Na-Cl facies, while the groundwater

Hydrology and
Earth System
Sciences
Discussions

379   facies close to the red point were Ca-HCO$_3$-Cl and Ca-Na-HCO$_3$. The groundwater facies found between

380   the blue and red points were the Ca-Na-HCO$_3$-Cl facies. As mentioned earlier, these were similar to the

381   study of Zghibi et al. (2014), who studied contamination in the Korba unconfined aquifer, which was

382   influenced by seawater intrusion. They showed a chemical analysis of water on the piper diagram and then

383   interpreted the results by creating the Theoretical Mixing Line (TML) of seawater and fresh water. They

384   found that groundwater showed paths of hydrochemical evolution along the TML line. The groundwater

385   facies can be changed from a Ca-SO$_4$ type to a Ca-Cl type to an Na-Cl type, and vice versa, from a Ca-SO4

386   type directly to an Na-Cl type, indicating that the chemical composition of groundwater is changed by a

387   cation exchange reaction.

388

389   *[Insert Figure 10]*

390

391   Figure 11 shows the relationship between the Na and Cl ions. The dominant ions in seawater are

392   Na and Cl, while the dominant ions in fresh water are Ca and HCO$_3$ (Appelo & Postma, 2005). Therefore,

393   the study of seawater intrusion has to focus on the dominant ions of seawater, which are Na and Cl ions.

394   The plotted graph comparing the Na and Cl ions found that it exhibited a strong correlation where the

395   groundwater samples fell on a 1:1 line with an R^2 of 0.941. This relationship suggests that both ions have

396   the same origin from seawater. The concentrations of Na and Cl depend on the degree of seawater intrusion

397   into the aquifer. From Figure 11, the groundwater can be divided into three groups. The first group, located

398   in the red circle, mainly consisted of samples in the Qcl aquifer that are severely influenced by seawater

399   intrusion. The groundwater types in this group showed Na-Cl and Ca-Na-Cl. The second group appeared

400   in the green circle, and consisted of groundwater samples from the PCms and Gr aquifers, which are

401   moderately influenced by seawater intrusion. The groundwater types in the second group showed Ca-Na-

402   HCO$_3$-Cl facies. The last group appeared in the blue circle and consisted of groundwater samples from the

403   deeper zone (when compared to the second group) of the PCms and Gr aquifers, which are slightly

404   influenced by seawater intrusion. The groundwater types in the last group showed Ca-HCO$_3$-Cl facies and

405   Ca-Na-HCO3 facies. These were consistent with the previous studies of Agoubi et al. (2013) and Zghibi et

406   al. (2014) that revealed the characteristics of groundwater chemistry influenced by seawater intrusion. They

407   found that groundwater influenced by seawater intrusion had dominant ions of Na and Cl. Therefore, when

408   plotting Na and Cl, both ions are well defined in the correlation where the groundwater sample falls on the

409   1:1 line, indicating that both ions come from the same source (seawater). Similarly, according to the ionic

410   ratio estimated from Cl/(HCO3 + CO3) and recommendation of Raghunath (1990), who suggested the ratio

411   of 2.8 as the threshold for indicating the saltwater intrusion, we found that more than 85% of groundwater

412   samples in the Qcl aquifer were moderately to highly contaminated due to seawater intrusion (Ebrahimi et

413   al., 2016).

414

415   *[Insert Figure 11]*

416

417   Furthermore, the study of Al-Agha and El-Nakhal (2004) found that by plotting the results of

418   groundwater samples on the piper diagram, phases of freshening and intrusion could be interpreted, but it

419   is difficult to recognize the sequence of facies in detail. Therefore, this research used the hydrochemical

420   facies evolution diagram (HFED) developed by Giménez-Forcada (2010) to describe the dynamic of

421   seawater intrusion. The percentage of major ions in the hydrochemical process associated with the dynamic

422   of seawater intrusion interface, consisting of Ca^{2+}, Na^+, HCO_3^-, SO_4^{2-}, Cl^-, was considered in the HFED.

423   Figure 12 shows that the red block (no. 4) is the Na-Cl facies (seawater), and the blue block (no. 13) is the

424   Ca-HCO_3 facies (fresh water). After plotting the percentage of ions on the diagram, it will generate a mixing

425   line between the fresh water and seawater to divide the phases of seawater intrusion. When the groundwater

426   samples appear above the mixing line, it represents the freshening phase, and if it falls below the mixing

427   line, this implies that it is during the intrusion phase. The results found that most of the samples fell close

428   to the mixing line (facies path 4–7–10–13), demonstrating mixing between seawater and fresh water. Some

429   samples fell in the intrusion phase (below the mixing line). In this initial phase, water gradually increases

430   the salinity along the facies path 13-14-15-16, which causes a reverse exchange, showing a Ca-Cl facies

431   (no. 16), which was not found in a groundwater sample in this facies. Finally, in this phase, water evolves

432   toward facies that are closer to seawater (Na-Cl facies) along facies path 16-12-8-4, and most samples in

433   this study were found in these groundwater facies. However, in this research, the groundwater sample fell

434   in Na-mixCl (no. 3), Na-mixHCO3 (no. 2), Na-HCO3 (no. 1), and MixNa-HCO3 (no. 5), which are

435   characteristic of the freshening process, and was not found in all groundwater samples.

436   Most samples that fell in the Na-Cl (no. 4) facies were groundwater samples collected from the Qcl

437   aquifer, and corresponded to the Na-Cl facies, which appeared in the piper diagram. This indicated that the

438   groundwater samples in the Qcl were severely influenced by seawater intrusion. Moreover, the groundwater

439   samples from the weathering PCms and Gr aquifers fell in the MixNa-Cl facie (no. 8) and MixCa-Cl (no.

440   12), which corresponded to the $Ca-Na-HCO_3-Cl$ facies in the piper diagram, indicated a moderate influence

441   of seawater intrusion. In addition, the groundwater samples from the PCms and Gr aquifers at deeper levels

442   (depth of 60–80 meters) showed the Ca- HCO3-Cl facies in the piper diagram and HFED fell in the Mix

443   Na-Cl facie (no. 8) and MixCa-Cl (no. 12). Even though it fell in the facies of fresh water in the HFED, it

444   was close to the mixing line; therefore, it was slightly influenced by seawater intrusion. These were

445   consistent with the study of Ghiglieri et al. (2012), who used HFED for depicting the salinization processes

446   in the coastal aquifers in Italy. They found that the sample plotted on HFED followed the succession of

447   facies along the mixing line, indicating that seawater and fresh water were slightly mixed or that the ionic

448   exchange process occurred. Moreover, they used the HFED results in comparison with the EC contour lines,

449   showing that seawater had intruded quite far inland. Najib et al. (2017) highlighted the succession of

450   different water facies developed between the intrusion and freshening phases by analysis on the HFED. The

451   formation of Na-HCO3 facies, which characterizes the last facies of the freshening phase, followed the

452   succession of Na-Cl, MixNa-MixCl, MixCa-MixCl, MixCa-MixHCO3, and Na-HCO3. Moreover, the

453   obtained HFED results allowed us to extend the intrusion process in the Holocene groundwater and accept

454   the fresh water recharge such as meteoric water and lateral recharge from rivers (Liu, 2017).

455

456   *[Insert Figure 12]*

457 *4.5. Multivariate Statistical Analysis*

458   4.5.1. Correlation matrix

459   In this study, the Pearson correlation technique was applied to assess the relationship between

460 various hydrochemical variables of the groundwater samples, which were measured in the field and

461 analyzed in the laboratory (see Table 2). The highlighted bold demonstrates the significant relationship at

462 $p < 0.05$. The high correlation of these parameters indicates that these cations/anions contributed to

463 mineralization in the aquifer systems. Chloride (Cl) is highly correlated with Na Na-Cl, r = 0.960, (SO_4^{2-}

464) Cl-SO4, r = 0.835, and (Br) Cl-Br, r = 0.857, implying that the groundwater system was influenced by

465 seawater intrusion (Askri et al., 2016). In general, the dissolution of halite may be investigated as the linear

466 relationship between Na and Cl ions (Hem, 1985). The total dissolved solid (TDS) had a significantly

467 positive correlation with EC TDS-EC, r = 0.963, (Na) TDS-Na, r = 0.934, (Cl) TDS-Cl, r = 0.923, (Br)

468 TDS-Br, r = 0.826 (SO₄) TDS-SO₄, r = 0.775 (and moderately correlated with Mg) TDS-Mg, r = 0.669,

469 (Ca) TDS-Ca, r = 0.435. Similarly, the EC was positively correlated with (Na) EC-Na, r = 0.910, (Cl) EC-

470 Cl, r = 0.914, (Br) EC-Br, r = 0.779, (SO₄) EC-SO4, r = 0.769, (as well as moderately correlated with

471 (Mg^{2+}) EC-Mg, r = 0.636, and (Ca^{2+}) EC-Ca, r = 0.425. These good correlations with EC implied that the

472 increase in salinity was caused from the groundwater mineralization (Moussa et al., 2011; Zghibi et al.,

473 2012). Calcium (Ca^{2+}) had a moderately positive correlation with Mg^{2+} Ca-Mg, r = 0.583, and was

474 moderately correlated with bicarbonate (HCO₃) (Ca-HCO₃, r = 0.422), implying the dissolution of calcite

475 and dolomite minerals from the geologic formation. Moreover, the good correlation between Mg and Na

476 (Mg-Na, r = 0705) indicated that the ion exchange was likely occurs during seawater intrusion.

477   4.5.2. Principal components analysis (PCA)

478   The varimax method used to rotate the parameters in the principal component analysis uses the

479 Kaiser criterion rotating with the varimax method. Therefore, all of parameters were classified into four

480 components (see Table 3). Each component included the values (bold) that represent a good correlation.

481 Table 4 shows the Eigen value of all parameters, and the four groups had Eigen values more than 1 and

482 cumulative variance was more than 80.35%. A total dissolved solid (TDS), EC, Mg^{2+}, Na^+, Cl^-, Br^-, SO_4^{2-}

483 were included in the first component that had the highest factor loading (6.13) and accounted for 47.17%

484 of the total variance. This factor, with a high positive loading, ranged from 0.757 to 0.965, probably

485 indicating the consequence of seawater intrusion in the study area. Therefore, factor 1 can be defined as the

486 "seawater intrusion factor". Similarly, the study of Ahmed et al. (2017) found that factor 1, which was

487 defined as the seawater intrusion impact, accounted for 66% of the total variance and consisted of these

488 following elements: EC, Cl, Na, SO4, K, Mg, Br, Sr, B, Cr, Co, Arsenic, and Selenium. The second

489 component had a factor loading of 1.60, accounting for 12.28% of the total variance. The component

490 showed the positive relationship between Ca^{2+} (0.62), F^- (0.63), and HCO_3 (0.77). This factor can be

491 expressed as the natural process when recharge water infiltrates into the groundwater system and water-

492 rock interaction occurs, which eventually releases Ca^{2+} and HCO_3^- in groundwater (Jiang et al., 2009). The

493 values of HCO_3 widely ranged from 19.52 mg/L to 189.5 mg/L, depending upon various geological

494 formations in this area. Fluoride is naturally released from the dissolution of fluorapatite and flurite, which

495 occurs in sedimentary and igneous rocks. According to Rama Rao (1982) and Heinrich (1948), they

496 revealed that fluorite was detected in granite, gneiss, and pegmatites. Moreover, due to the similarity charge

497 and radius, fluoride can substitute the hydroxide ions via water-rock interaction. Similar to Ca and HCO_3,

498 fluoride (F) in groundwater can be inferred from the weathering of rocks in this area. The third component

499 consisting of K^+ and Fe showed positive loadings in the range of 0.7–0.81 and the factor loading was

500 1.448 or 11.14% of the total variance. Through the weathering of igneous rocks, K can be mainly released

501 from potassium feldspar into the groundwater (Kim et al., 2004) and Fe represents the natural dissolution

502 of rocks and minerals via water-rock interaction. The last component consists of only pH showing the low

503 factor loading (1.27) or 9.78% of the total variance. These parameters might be the result of various dynamic

504 hydro-geochemical processes in the area such as seawater intrusion, recharge, water-rock interaction, etc.

505 In addition, all variables were plotted in rotated space in Figure 13 to clearly demonstrate the separation of

506 the four components.

507

508 *[Insert Table 2]*

Hydrology and
Earth System
Sciences
Discussions

Open Access

EGU

509   *[Insert Table 3]*

510   *[Insert Table 4]*

511   *[Insert Figure 13]*

512

513   *4.6. Integrated Interpretation of VES and EC Results*

514   VES data has a limitation when further interpreting seawater intrusion as there are many factors

515   that show resistivity values of <5 Ωm in coastal aquifers. Therefore, the results of the hydrochemical

516   analysis and EC value needed to be interpreted with the VES data to overcome this limitation and to further

517   elucidate the seawater intrusion effect. The VES sections were overlaid on the EC map of the Qcl aquifer,

518   which was severely affected by seawater intrusion, then obtained the extent of intrusion as shown in Figure

519   16. The zone with resistivity values <5 Ωm were considered to be the seawater intrusion area. Furthermore,

520   the EC map showed the location of high EC (>1500 μs/cm), corresponding to the location of low resistivity

521   values (<5 Ωm).

522   From this relationship, it can be concluded that the Qcl aquifer was highly influenced by seawater

523   intrusion with resistivity values in the range of 0–10 Ωm, especially in the upper part of the area. The

524   boundary line is shown in Figure 14. Section A-A' was influenced by seawater intrusion about 3 km inland,

525   where the first kilometer from the coast line was highly influenced with resistivity values <5 Ωm, while the

526   last two kilometers were moderately influenced and represented brackish water with resistivity values

527   ranging 5–10 Ωm. Section B-B' was influenced by seawater intrusion about 5 km inland, where the first 2

528   km from the coastal line were highly influenced with resistivity values of <5 Ωm, while the last 3 km were

529   moderately influenced with resistivity values ranging from 5–10 Ωm. Section C-C' was influenced by

530   seawater intrusion about 4.7 km inland where the first 3.2 km from the coast line was highly influenced

531   with resistivity values of <5 Ωm, while the following 1.5 km were moderately influenced with resistivity

532   values of 5–10 Ωm. Section D-D' was influenced by seawater intrusion about 8 km inland where the first

533   4 km from the coast line was highly influenced with resistivity values of <5 Ωm, while the next 4 km was

534   moderately influenced with resistivity values of 5–10 Ωm. As shown from the geophysical and

535   hydrochemical results, the levels of seawater intrusion could be classified into three zones by using the

536   criteria shown in Table 5.

537

538   *[Insert Figure 14]*

539   *[Insert Table 5]*

540

541   **5. CONCLUSIONS**

542   In this research, 80 VES surveys were conducted using a Schlumberger configuration integrated

543   with the hydrochemical analysis of 58 groundwater samples to indicate seawater intrusion into coastal

544   aquifers. Four pseudo cross-sections were generated from the 80 VES data. These were in a good agreement

545   with those obtained from the hydrogeological data and lithologic data in the study area. The resistivity map

546   at different depths, generated from the VES data, successfully revealed the interaction of seawater and

547   freshwater along the coast line. The geophysical results found that seawater mainly intruded in the Qcl

548   aquifer. The resistivity values of <5 Ωm were found at a depth of approximately 50 m. However, the VES

549   is limited when evaluating the seawater intrusion in highly contaminated aquifer located close to the coast

550   line. Therefore, the evaluation of seawater intrusion in coastal areas with VES data needs the assistance of

551   hydrochemical and hydrogeological data to describe the seawater intrusion more accurately. According to

552   the hydrochemical analysis of 58 groundwater samples, five types of groundwater facies (Ca-Na-HCO3,

553   Ca-HCO3-Cl, Ca-Na-HCO3-Cl, Ca-Na-Cl and Na-Cl) were noticed, which were dependent upon aquifer

554   types and depths. Na-Cl facies were typically found in the Qcl aquifer, corresponding to the resistivity

555   values of <5 Ωm. As the geophysical and hydrochemical results showed, the levels of seawater intrusion

556   could be classified into three zones depending on the degree of seawater intrusion. As a suggestion of this

557   research, groundwater samples should be periodically collected from at least two periods to analyze the

558   dynamic and evolution of seawater intrusion. The VES investigation should be concerned with the distance

559   between the VES survey point and the VES point near the coast line as the depth of survey cannot penetrate

560   through the highly seawater contaminated groundwater. Moreover, the lithologic data for aquifers that have

561 a lot of clay components are required to interpret the results more accurately. In the future, when this area

562 needs to use the groundwater resources, people should use groundwater in the rock aquifers (PCms and Gr

563 aquifers) at depths of higher than 70 meters. The proper criteria for selecting the study area of seawater

564 intrusion should consider the following: groundwater demand in the area, ecological and hydrogeological

565 characteristics, and the amount of groundwater recharge needed to prevent problems that may occur from

566 a large amount of groundwater pumping in the future.

567

577

578

579

580

581

582

583

584

Hydrology and
Earth System
Sciences
Discussions

Open Access

EGU

585   **REFERENCES**

586   Abderamane H, Razack M, Vassolo, S., 2012. Hydrogeochemical and isotopic characterization of the

587   groundwater in the Chari-Baguirmi depression, Republic of Chad. Environ. Earth Sci. 69, 2237-2350.

588   Agoubi, B., Kharroubi, A., Abichou, T., Abida, H., 2013. Hydrochemical and geoelectrical investigation

589   of Marine Jeffara aquifer, southeastern Tunisia. Appl. Water Sci. 3, 415-429.

590   Ahmed, A.H., Rayaleh, W.E., Zghibi, A. and Ouddane, B., 2017. Assessment of chemical quality of

591   groundwater in coastal volcano sedimentary aquifer of Djibouti, Horn of Africa. J. Afr. Earth Sci. 131,

592   284-300.

593   Al-Agha, M.R., El-Nakhal, H.A., 2004. Hydrochemical facies of groundwater in the Gaza Strip, Palestine.

594   Hydrolog. Sci. J. 49(3), pp. 359.

595   Appelo, C.A.J., Postma, D., 2005. Geochemistry, groundwater and pollution (2nd ed.). Boca Raton: CRC

596   press.

597   Askri, B., Ahmed, A.T., Al-Shanfari, R.A., Bouhilla, R., Al-Farisi, K.B.K., 2016. Isotopic and geochemical

598   identifications of groundwater salinization processes in Salalah coastal plain, Sultanate of Oman 76,

599   243-255.

600   Bear, J., 1999. Conceptual and mathematical modeling in Seawater intrusion in coastal aquifers. Springer

601   Netherlands, pp. 127-161.

602   Bobachev, A.A., 2003. IPI2Win software. Available from: <http//geophys.geol.msu.ru/ipi2win.htm>.

603   Cimino, A., Cosentino, C., Oieni, A., Tranchina, L., 2008. A Geophysical and geochemical approach for

604   seawater intrusion assessment in the Acquedolci coastal aquifer (Northern Sicily). Environ. Geol. 55,

605   1473-1482. http://dx.doi.org/10.1007/s00254-007-1097-8.

606   Department of Groundwater Resources (DGR), 2001. Groundwater Guide Manual Book, Phetchaburi

607   Province. Department of Groundwater Resources.

608   Department of Groundwater Resources, 2015. The project of hydrogeological survey and the potential

609   assessment of groundwater in water shortage areas and repeated drought areas in Phetchaburi and

610   Prachuap Khiri Khan basin.

Hydrology and
Earth System
Sciences
Discussions

Open Access

611   Department of Mineral Resources (DMR), 2014. Geology of Thailand. Department of Mineral Resources:

612   Bureau of Geological Survey, Department of Mineral Resources, Bangkok, Thailand.

613   Ebrahimi, M., Kazemi, H., Ehtashemi, M., Rockaway, T.D., 2016. Assessment of groundwater quantity

614   and quality and seawater intrusion in the Damaghan basin, Iran. Chemie der Erde 76, 227-241.

615   Essink, G.H.P.O., 2001. Improving fresh groundwater supply-problems and solutions. Ocean Coast.

616   Manage. 44, 429-449. http://dx.doi.org/10.1016/s0964-5691(01)00057-6.

617   Fadili, A., Najib, S., Mehdi, K., Riss, J., Malaurent, P., Makan, A., 2017. Geoelectrical and hydrochemical

618   study for the assessment of seawater intrusion evolution in coastal aquifers of Oualidia, Morocco. J.

619   Appl. Geophys. 146, 178-187.

620   Galloway, W.E., Kaiser, W.R., 1980. Catahoula formation of the Texas coastal plain: origin, geochemical

621   evolution, and characteristics of uranium deposits, Univ. Texas, Austin, Bur. Econ. Geol., Rep. Invest.

622   100, pp. 81.

623   George, N.J., Ibanga, J.I., Ubom, A.I., 2015. Geoelectrohydrogeological indices of evidence of ingress of

624   saline water into freshwater in parts of coastal aquifers of Ikot Abasi, southern Nigeria. J. Afr. Earth

625   Sci. 109, 37-46.

626   Ghiglieri, G., Carletti, A., Pittalis, D., 2012. Analysis of salinization processes in the coastal carbonate

627   aquifer of Porto Torres (NW Sardinia, Italy). J. Hydrol. 432-433, 43-51.

628   Giménez-Forcada, E., 2010. Dynamic of seawater interface using hydrochemical facies evolution diagram.

629   Ground Water 48(2), 212-216.

630   Gopinath, S., Srinivasamoorthy, K., 2015.Application of geophysical and hydrogeochemical tracers to

631   investigate salinization sources in Nagapatinam and Karaikal coastal aquifers, South India. Aquat.

632   Procedia. 4, 65-71.

633   Heinrich, E.W.M., 1948. Fluorite-rare earth mineral pegmatites of Chaffee and Fremont Counties, Colorado

634   University of Michigan, Ann Arbor, Michigan. Am Mineral 33, 64–75.

635   Hem, J.D., 1985. Study and interpretation of the chemical characteristics of naturalwater (3d ed.), U.S.

636   Geological Survey, Water Supply Paper 2254.

Hydrology and
Earth System
Sciences
Discussions

637   Jiang, Y., Wu, Y., Groves, C., Yuan, D., and Kambesis, P., 2009. Natural and anthropogenic factors

638   affecting the groundwater quality in the Nandong karst underground river system in Yunan, China. J.

639   Contam. Hydrol. 109, 49-61.

640   Kang, M., Jackson, R.B., 2016. Salinity of deep groundwater in California: Water quantity, quality, and

641   protection. Proc. Natl. Acad. Sci. USA 113 (28), 7768-7773.

642   Kaya, M.A., Özürlan, G., Balkaya, Ç., 2015. Geoelectrical investigation of seawater intrusion in the coastal

643   urban area of Canakkale, NW Turkey. Environ. Earth Sci. 73, 1151-1160.

644   Kazakis, N., Pavlou, A., Vargemezis, G., Voudouris, K.S., Soulios, G., Pliakas, F., Tsokas, G., 2016.

645   Seawater intrusion mapping using electrical resistivity tomography and hydrochemical data. An

646   application in the coastal area of eastern Thermaikos Gulf, Greece. Sci. Total Environ. 543, 373-387.

647   Kim, K., Rajmohan, N., Kim, H.J., Hwang, G.S., Cho, M.J., 2004. Assessment of groundwater chemistry

648   in a coastal region (Kunsan, Korea) having complex contaminant sources: a stoichiometric approach.

649   Environ. Geol. 46, 763–774.

650   Kouzana, L., Benassi, R., Ben Mammou, A., Sfar Felfoul, M., 2010. Geophysical and hydrochemical study

651   of the seawater intrusion in Mediterranean semiarid zones, case of the Korba coastal aquifer (Cap-Bon,

652   Tunisia). J. Afr. Earth Sci. 58(2), 242-254. https://dx.doi.org/10.1016/j.jafrearsci.2010.03.005.

653   Land Developement Department, 2011. Land use Map of Phetchaburi.

654   Liu, S., Tang, Z., Gao, M., Hou, G., 2017. Evolutionary process of saline-water intrusion in Holocene

655   and Late Pleistocene groundwater in southern Laizhou Bay. Sci. Total Environ. 607-608, 586-599.

656   https://doi.org/10.1016/j.scitotenv.2017.06.262.

657   Mas-Pla, J., Ghiglieri, G., Uras, G., 2014. Seawater intrusion and coastal groundwater resources

658   management. Examples from two Mediterranean regions: Catalonia and Sardinia. Contrib. Sci. 10, 171-

659   184.

660   McInnis, D., Silliman, S., Boukari, M., Yalo, N., Orou-Pete, S., Fertenbaugh, C., Fayomi, H., Sarre, K.,

661   2013. J. Hydrol. 505, 335-345.

662   Morgan, L.K., Werner, A.D., 2015. A national inventory of seawater intrusion vulnerability for Australia.

663   J. Hydrol. Regional Studies 4, 686-698.

664   Moussa, A.B., Zouari, K., Valles, V., Jlassi, F., 2012. a Hydrogeochemical analysis of groundwater

665   pollution in an irrigated land in cap bon peninsula, north-eastern Tunisia. Arid Land Res. Manag.. 26,

666   1-14.

667   Najib, S., Fadili, A., Mehdi, K., Riss, J., Makan, A., 2017. Contribution of hydrochemical and geoelectrical

668   approaches to investigate salinization process and seawater intrusion in the coastal aquifers of Chaouia,

669   Morocco. J. Contam. Hydrol. 198, 24-36.

670   Raghunath, H.M., 1990. Groundwater. Wiley Eastern Ltd., New Delhi.

671   Rama Rao, N.V., 1982. Geochemical factors influencing the distribution of fluoride in the rocks, soil and

672   water sources of Nalgonda district. AP thesis, Osmania University, Hyderabad.

673   Ravindran, A.A., 2013. Coastal-zone shallow-aquifer characterization study using geoelectrical and

674   geochemical methods in Zirconium Complex, Atomic Energy, Pazhayakayal, Thoothykudi, India. Russ

675   Geol. Geophys. 54(12), 1529-1538. https://doi.org/10.1016/j.rgg.2013.10.021.

676   Ros, S.E.M., Zuurbier, K.G., 2017. The Impact of Integrated Aquifer Storage and Recovery and Brackish

677   Water Reverse Osmosis (ASRRO) on a Coastal Groundwater System. Water 9, 273.

678   Sabet, M.A., 1975. Vertical electrical resistivity soundings to locate groundwater resources: a feasibility

679   study. Department of Geophysical Sciences 63.

680   Samouëlian, A., Cousin, I., Tabbagh, A., Bruand, A., Richard, G., 2005. Electrical resistivity survey in soil

681   science: a review. Soil Till. Res. 83(2), 173-193. https://doi.org/10.1016/j.still.2004.10.004.

682   Sherif, M., Mahmoudi, A.E., Garamoon, H., Kacimov, A., Akram, S., Ebraheem, A., Shetty, A., 2006.

683   Geoelectrical and hydrogeochemical studies for delineating seawater intrusion in the outlet of Wadi

684   Ham, UAE. Environ. Geol. 49(4), 536-551.

685   Shi, L., Jiao, J.J., 2014. Seawater intrusion and coastal aquifer management in China: a review. Environ.

686   Earth Sci. 72, 2811-2819.

687   Song, S., Lee, J., Park, N., 2006. Use of vertical electrical soundings to delineate seawater intrusion in a

688   coastal area of Byunsan, Korea. Environ. Geol. 52(6), 1207-1219.

689   Telford, W.M., Geldart, L.P., Sheriff, R.E., 1990. Applied Geophysics. Cambridge University Press. pp.

690   792.

691   Van Dam, J.C., Meulenkamp, J.J., 1967. Some results of the geo-electrical resistivity method in

692   groundwater investigations in the Netherlands. Geophys. Prospect 15(1), 92-115.

693   Werner, A.D., Bakker, M., Post, V.E.A., Vandenbohede, A., Lu, C., Ataie-Ashtiani, B., Simmons, C.T.,

694   Barry, D.A., 2013. Seawater intrusion processes, investigation and management: Recent advances and

695   future challenges. Adv. Water. Resour. 51, 3-26. DOI:10.1016/j.advwatres.2012.03.004.

696   Zarroca, M., Bach, J., Linares, R., Pellicer, X.M., 2011. Electrical methods (VES and ERT) for identifying,

697   mapping and monitoring different saline domains in a coastal plain region (Alt Emporda, Northern

698   Spain). J. Hydrol. 409, 407-422.

699   Zghibi, A., Zouhri, L., Tarhouni, J., Kouzana, L., 2012. Groundwater mineralization processes in

700   Mediterranean semi-arid systems (Cap-Bon, North east of Tunisia): hydrogeological and geochemical

701   approaches. Hydrol. Process. http://dx.doi.org/10.1002/hyp.9456.

702   Zghibi, A., Merzougui, A., Zouhri, L., Tarhouni, J., 2014. Understanding groundwater chemistry using

703   multivariate statistics techniques to the study of contamination in the Korba unconfined aquifer system

704   of Cap-Bon (North-east of Tunisia). J. Afr. Earth Sci. 89, 1-15.

705   Zohdy, A.A., Eaton, G.P., Mabey, D.R., 1974. Application of surface geophysics to ground-water

706   investigations. US Government Printing Office.

707

708

709

710

711

712

Hydrology and
Earth System
Sciences
Open Access
Discussions
EGU

Table 1 Hydrochemical analysis of groundwater samples

Sample No.	Well No.	TDS (mg/l)	EC (µs/cm)	K (mg/L)	Fe (mg/L)	Ca (mg/L)	Mg (mg/L)	Na (mg/L)	F (mg/L)	Cl (mg/L)	Br (mg/L)	No3 (mg/L)	SO4 (mg/L)	CO3 (mg/L)	HCO3 (mg/L)	%A
W1	MU287	205	1000	12.25	N/D	35.4	5.6	95.8	0.347	82.12	0.839	0.64	7.16	25.2	51.24	23.105
W2	5608C006	1307	1951	4.5	0.008	100.6	18.9	159	2.033	215.075	1.671	3.857	24.2	67.2	136.64	9.162
W3	5408D026	773	1155	5.7	N/D	98.95	17.7	109.75	2.901	89.2	1.678	1.501	12.16	64.8	131.76	22.247
W4	MU747	607	905	8.4	N/D	48.4	13.3	82	1.184	128.92	1.368	0.353	0.708	39.6	80.52	7.185
W5	PCR9	718	1071	13.45	N/D	49.65	17.4	64.2	1.254	79.53	1.84	N/D	0.223	63.6	129.32	4.13
W6	C629	905	1348	16.05	N/D	48.01	18.2	129.6	1.195	219.525	1.535	7.9	13.2	22.4	72.3	5.202
W7	MU134	739	1105	14.75	N/D	41.9	9	115.5	0.823	229.5	1.475	0.308	0.054	18	36.6	3.402
W8	Private	761	1137	11	N/D	45.3	12	137.75	1.806	215.4	2.098	N/D	1.763	18	118.6	4.783
W9	Private	781	1170	7.7	N/D	58.95	12.9	40.2	3.18	84.84	1.94	2.889	4.928	N/D	132.6	9.927
W10	MU753	602	1123	9.15	0.147	17.6	8.7	54.6	0.134	119.88	1.065	0.033	9.939	N/D	48.8	-2.149
W11	Private	825	1360	17.45	N/D	46.9	18.5	127.25	1.239	216.475	1.919	10.52	9.615	N/D	141.52	2.452
W12	q1642	781	1166	13.35	N/D	69.4	20.5	115	1.265	167.6	2.566	7.367	5.736	N/D	119.56	17.754
W13	DCD14827	805	1230	6.55	N/D	70.6	34	103.2	1.462	169.975	2.008	1.449	16.3	N/D	112.24	21.629
W14	5508C019	757	1130	4.75	N/D	58.95	34	92.2	1.192	164.94	2.791	N/D	2.402	52.8	107.36	9.137
W15	DCD14809	779	1162	6.8	0.548	68.75	19.7	90.6	0.833	180.95	2.228	0.149	0.046	N/D	145.9	9.978
W16	Private	1650	879	43	N/D	86.15	24.6	241	0.513	336.28	3.654	28.88	44	N/D	158.6	8.641
W17	MU135	397	594	20.8	N/D	45.35	11.7	32	0.134	56.14	1.583	0.183	12.83	N/D	158.6	7.142
W18	Private	1720	3024	4.75	N/D	168.4	27.8	199.6	3.115	400.88	3.589	10.64	84.96	60	122	4.461
W19	Private	801	1196	14.55	N/D	70.3	18.2	40.5	1.25	72.8	2.996	9.478	12.32	N/D	182.7	8.826
W20	ND	591	883	4.65	N/D	81.2	12.1	32.4	0.969	69.4	2.758	1.245	12.27	N/D	189.5	9.745
W21	5408D022	782	1168	16.3	0.009	45.65	18.4	133	1.156	252	2.984	3.334	10.24	N/D	122	2.255

7

Table 1 Hydrochemical analysis of groundwater samples (continue)

Sample No.	Well No.	TDS (mg/l)	EC (µs/cm)	K (mg/L)	Fe (mg/L)	Ca (mg/L)	Mg (mg/L)	Na (mg/L)	F (mg/L)	Cl (mg/L)	Br (mg/L)	No3 (mg/L)	SO₄ (mg/L)	CO₃ (mg/L)	HCO₃ (mg/L)	%A
W22	DCD14772	556	830	8.95	0.103	50	13.8	107.6	2.728	204.78	2.198	0.034	4.215	N/D	102.48	6.208
W23	5608C045	375	562	10.05	N/D	61.15	9.6	44.4	0.269	135.2	1.684	0.074	26.3	N/D	70.4	4.433
W24	MU563	900	1347	6.55	0.056	71.05	32.6	122.5	1.588	279.5	3.156	3.561	65.3	N/D	68.32	4.982
W25	MU564	843	1130	6.05	N/D	93.9	47.2	198.8	1.234	477.8	4.536	1.061	71.75	N/D	68.32	3.63
W26	5408D011	195	292	14.1	N/D	15.65	4	33	1.944	34.6	0.836	12.02	1.287	N/D	21.96	13.368
W27	Q167	494	739	19.55	0.048	57.3	8.7	68	1.955	129.8	1.578	2.093	0.921	N/D	84.8	14.824
W28	q1607	391	584	12.7	0.879	45.95	9.8	62	1.934	125.6	1.664	0.183	0.031	N/D	94.6	9.056
W29	Private	267	400	23.65	0.925	18.9	3.4	24.8	2.219	50.4	0.754	0.973	0.185	28.8	58.56	-8.031
W30	MU283	420	627	16.35	0.209	45.4	7.1	42.9	2.154	87.6	1.541	0.567	6.204	N/D	124.6	4.608
W31	PCR10	460	687	9.05	N/D	45.15	11.7	87.6	2.492	100.5	1.68	0.072	8.604	N/D	70.76	26.942
W32	DCD14768	503	375	18.4	2.73	44.6	12.3	40.1	1.551	64.3	2.021	0.086	0.061	20.1	122	9.68
W33	MU348	507	757	10.05	N/D	56.3	13.1	70.2	1.308	130.15	1.946	5.401	3.659	N/D	132.5	6.632
W34	MU363	548	1015	8.65	N/D	51.4	13.1	118.2	1.199	259.6	0.953	1	8.577	N/D	62.3	2.377
W35	MU571	762	1138	15.65	0.069	45.6	17.2	134.6	1.001	269.8	2.659	1.949	9.96	N/D	82.6	3.334
W36	MU332	649	1002	57.3	N/D	59.35	21.8	82	0.288	178.6	2.225	N/D	24.2	N/D	112.24	14.043
W37	MU359	780	1267	58.3	1.104	58.75	17.8	123.4	0.199	247.95	3.282	0.316	29.25	N/D	97.6	9.942
W38	MU557	565	848	43.1	1.721	125.55	36.6	215.5	0.307	380.24	3.959	0.129	131.56	N/D	122	12.171
W39	MU458	239	357	15.1	0.387	15.5	5.9	33	0.17	64.3	0.812	1.052	2.281	N/D	34.6	10.366
W40	5608C007	426	631	12.2	N/D	41.8	11.4	80	1.059	100.6	1.608	0.058	1.647	N/D	31.72	33.522
W41	MU361	559	834	11.2	N/D	49	13.6	87.6	4.325	97.3	1.711	4.303	24.43	51.6	104.92	4.512
W42	MU335	454	677	15.8	N/D	44.85	11.1	75.8	1.342	86.7	1.778	1.63	3.014	N/D	75.64	27.902
W43	MU549	621	929	14.15	N/D	76.1	18.9	93.8	1.975	154.3	2.084	8.536	5.307	51.6	104.92	7.02
W44	DCD14766	753	1124	12	0.007	58.35	16.4	82.4	2.31	170.425	1.806	0	2.524	52.8	107.36	-1.354

7

715

30

Hydrology and
Earth System
Sciences

Open Access

EGU

Discussions

7

Table 1 Hydrochemical analysis of groundwater samples (continue)

Sample No.	Well No.	TDS (mg/l)	EC (µs/cm)	K (mg/L)	Fe (mg/L)	Ca (mg/L)	Mg (mg/L)	Na (mg/L)	F (mg/L)	Cl (mg/L)	Br (mg/L)	No3 (mg/L)	SO4 (mg/L)	CO3 (mg/L)	HCO3 (mg/L)	%A
W45	AFD8794	531	793	12.25	1.665	36.2	3.6	60.9	1.984	62.26	0.64	6.487	10.9	40.8	82.96	-0.991
W46	MU588	254	379	8.25	0.019	24.75	7.8	32.4	0.743	15.486	1.05	0.042	5.706	16	54.2	27.687
W47	DCD14773	649	970	12.95	N/D	61.3	16.8	89.6	1.705	134.6	1.933	14.78	8.539	N/D	136.64	8.798
W48	MU578	629	939	17.05	N/D	70.9	18.3	85.2	1.564	53.18	2.169	16.88	10.12	N/D	87.84	35.666
W49	DOH11441	340	514	29.35	0.062	24.6	12	42.1	0.665	60.72	1.104	0.467	8.423	36	72.4	5.378
W50	MU331	660	986	20.95	0.066	66.25	22	92.4	0.771	184.2	2.135	0.356	3.86	39.6	80.52	9.848
W51	MU586	762	1138	13.3	N/D	72.9	12.9	84.3	1.96	171.1	2.244	2.601	4.256	14	122	7.023
W52	MU697	397	598	3.25	N/D	65.2	10.2	64.2	0.099	100.4	1.085	1.06	11.8	40	89.4	7.876
W53	q1605	2090	3120	4.85	N/D	214.55	30.5	288.4	N/D	920.9	4.776	9.142	74.8	36	73.2	-8.29
W54	PCR16	3580	5360	14	N/D	38.05	37.8	665	0.247	1489.2	6.372	3.524	167.4	50.4	102.48	-17.723
W55	q86	1920	2860	9.35	N/D	73.5	31.4	284.6	0.408	662.2	4.611	N/D	24.2	40.1	117.12	-8.603
W56	q88	2920	4360	15.15	N/D	82.2	41.8	541	0.294	935.6	6.101	N/D	160.6	64.8	131.76	-3.928
W57	C545	207	310	10.5	N/D	60.35	12.5	56.4	1.206	92.16	2.565	1.012	12.34	62.4	126.88	-2.354
W58	Private	784	1169	7.15	N/D	14.95	3.8	15.2	0.193	43.46	0.638	0.122	0.119	N/D	19.52	10.028
Seawater		37675.2	53821.7	396.931	0.488	841.1	1083.43	11106.3	9.7944	21192.1	37.7172	N/D	2793.78	70.3998	143.142	-2.78

* Detection limit of IC standard (anion) = 10 ppm, AAS standard for Ca^{2+} = 5 ppm, Mg^{2+} = 0.25 ppm, Na^+ = 0.5 ppm, K^+ = 1 ppm and Fe = 3 ppm

** Acceptable % error balance is less than ±10 % (ALS Environmental)

***N/D = Not detected

717

31

718 **Table 2** Pearson's correlation coefficient)R^2 (between the physiochemical and hydro chemical parameter from 58 groundwater
719 samples.

Variables	pH	TDS	EC	K^+	Fe	Ca^{2+}	Mg^{2+}	Na^+	F^-	Cl^-	Br^-	SO_4^{2-}	alkalinity
pH	1.000												
TDS	-0.145	1.000											
EC	-0.177	**0.963**	1.000										
K^+	0.032	-0.035	-0.118	1.000									
Fe	0.056	-0.156	-0.189	0.324	1.000								
Ca^{2+}	-0.249	**0.435**	**0.425**	-0.067	-0.050	1.000							
Mg^{2+}	-0.227	**0.669**	**0.636**	0.052	-0.093	**0.583**	1.000						
Na^+	-0.196	**0.934**	**0.910**	0.046	-0.097	**0.362**	**0.705**	1.000					
F^-	0.216	-0.187	-0.169	-0.295	-0.010	0.038	-0.164	-0.237	1.000				
Cl^-	-0.162	**0.923**	**0.914**	0.003	-0.094	**0.420**	**0.696**	**0.960**	-0.290	1.000			
Br-	-0.072	**0.826**	**0.779**	0.115	-0.048	**0.564**	**0.849**	**0.847**	-0.223	**0.857**	1.000		
SO_4^{2-}	-0.165	**0.775**	**0.769**	0.141	0.058	**0.472**	**0.728**	**0.863**	-0.233	**0.835**	**0.817**	1.000	
alkalinity	-0.104	**0.378**	**0.342**	-0.046	-0.015	**0.422**	**0.346**	0.282	0.222	0.206	**0.399**	0.229	1.000

720 Values in the highlighted bold indicate a relationship between two parameters with a significance level at 0.05 ($P<0.05$)
721
722
723
724
725
726
727
728
729
730
731
732
733
734
735
736
737
738
739
740
741
742
743
744
745
746
747
748
749

750 **Table 3** Rotated component matrix dividing variables into four groups
751

	Component			
	1	2	3	4
pH	-0.063	-0.064	-0.82	**0.916**
TDS	**0.943**	0.114	-0.122	-0.031
EC	**0.922**	0.097	-0.201	-0.051
K^+	0.065	-0.192	**0.810**	-0.057
Fe	-0.111	0.120	**0.786**	0.105
Ca^{2+}	0.415	**0.616**	0.014	-0.360
Mg^{2+}	**0.757**	0.294	0.065	-0.251
Na^+	**0.965**	0.018	-0.029	-0.069
F^-	-0.298	**0.630**	-0.248	0.439
Cl^-	**0.968**	-0.021	-0.048	-0.072
Br^-	**0.907**	0.228	0.116	-0.064
SO_4^{2-}	**0.884**	0.090	0.172	-0.103
alkalinity	0.254	**0.771**	0.016	-0.055

752 The values bold demonstrate highly relationship in each component .
753 Rotation Method :Varimax with Kaiser Normalization.
754
755
756
757
758
759
760
761
762
763
764
765
766
767
768
769
770
771
772
773
774
775
776
777
778
779
780
781
782
783
784
785

Hydrology and
Earth System
Sciences
Open Access
Discussions
EGU

Table 4 Total variance explained of various factors .

Component	Initial Eigenvalues			Extraction sums of squared Loadings			Rotation sums of squared loadings		
	Total	%of Variance	Cumulative %	Total	%of Variance	Cumulative %	Total	%of Variance	Cumulative %
1	6.486	49.892	49.892	6.486	49.892	49.892	6.132	47.166	47.166
2	1.602	12.325	62.217	1.602	12.325	62.217	1.596	12.277	59.443
3	1.262	9.708	71.926	1.262	9.708	71.926	1.448	11.142	70.585
4	1.096	8.434	80.359	1.096	8.434	80.359	1.271	9.775	80.359
5	0.715	5.503	85.863						
6	0.629	4.840	90.702						
7	0.485	3.733	94.436						
8	0.340	2.618	97.053						
9	0.180	1.387	98.441						
10	0.097	0.749	99.190						
11	0.054	0.415	99.605						
12	0.033	0.257	99.862						
13	0.018	0.138	100.000						

1   **Table 5.** The levels of seawater intrusion with resistivity and EC values
2

Level of seawater intrusion	Resistivity (Ωm)	EC (μs/cm)	Groundwater Facies
Extremely	< 5	>1500	Na-Cl
Moderately	5-10	1000-1500	Na-Cl, Ca-Na-Cl , Ca-Na-HCO3-Cl, Ca-Na-HCO3, Ca-HCO3-Cl
Slightly	>10	<1000	Ca-Na-Cl ,Ca-Na-HCO3, Ca-Na-HCO3-Cl, Ca-HCO3- Cl

3
4
5
6
7
8
9
10
11
12
13
14
15
16
17
18
19
20
21
22
23
24
25
26
27
28
29
30
31
32
33
34
35
36
37
38
39
40
41
42
43

44

45

46

47

48

49 **Figure captions**

50 **Figure 1a.** Study area map including VES points, sample collected well and location of four cross-

51 section lines A-A', B-B', C-C', and D-D'.

52 **Figure 1b.** Land use map of the study area (Land Development Department, 2011).

53 **Figure 2.** Geological map in the study area (adapted from the Department Mineral Resources 2007).

54 **Figure 3.** Hydrological map in the study area (adapted from the Department of Groundwater Resources

55 (DGR), 2014).

56 **Figure 4.** Schlumberger configuration.

57 **Figure 5.** (**a**) Apparent resistivity type curve (type H) for three horizontal layers. (**b**) IPI2WIN

58 interpretation of VES St-25.

59 **Figure 6.** Pseudo cross-section lines A-A', B-B', C-C' and D-D'.

60 **Figure 7.** Resistivity value versus lithologic-log from the pseudo cross-section lines D-D' (well Q168

61 versus VES St 47 and well PW 7962versus VES St 34).

62 **Figure 8.** Geological cross-section lines as follows: (**a**) A-A'; (**b**) B-B'; (**c**) C-C'; and (**d**) D-D'.

63 **Figure 9.** Apparent resistivity map for AB/2 equals: (**a**) 5 meters; (**b**) 10 meters; (**c**) 30 meters; (**d**) 50

64 meters; (**e**) 70 meters; (**f**) 100 meters; (**g**) 150 meters; and (**h**) 200 meters.

65 **Figure 10.** Hydrochemical analysis of groundwater sample plotted in the piper diagram.

66 **Figure 11.** The relationship plotting between Na and Cl concentration (in meq/L) in the groundwater

67 samples collected from different aquifers.

68 **Figure 12.** Hydrochemical Facies Evolution Diagram (HFED) for depicting the salinization process in

69 this area.

70 **Figure 13.** A component plot in rotated space.

71 **Figure 14.** The boundary of seawater intrusion in the Qcl aquifer, based on the EC contour map

72 superimposed on the resistivity map.

73

74

75

76

77

78

79

80

81

Figure 1a.

Figure 1b.

109

Figure 2.

110

111

Hydrology and
Earth System
Sciences
Discussions

Open Access

112
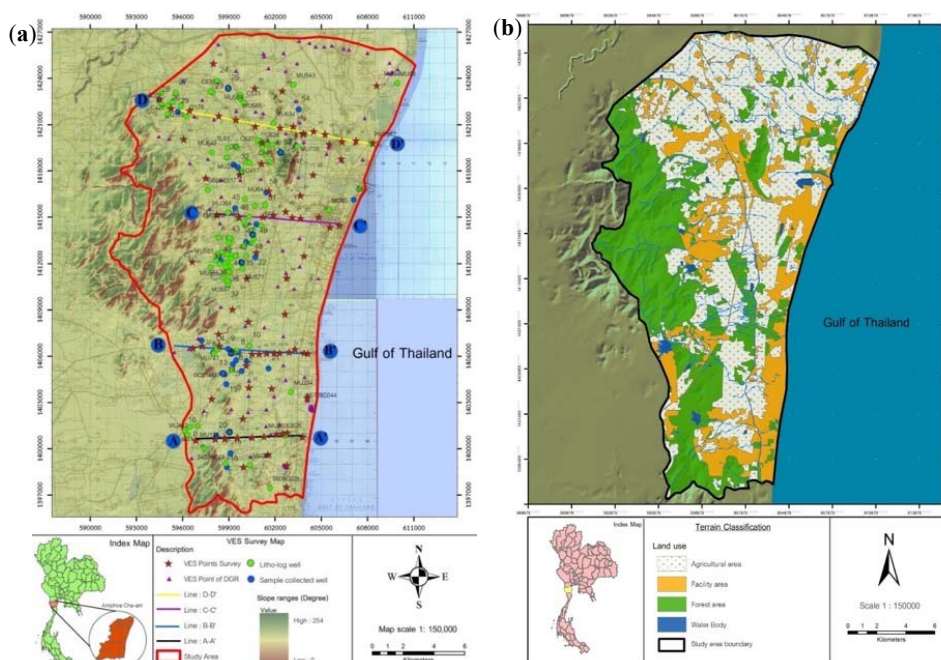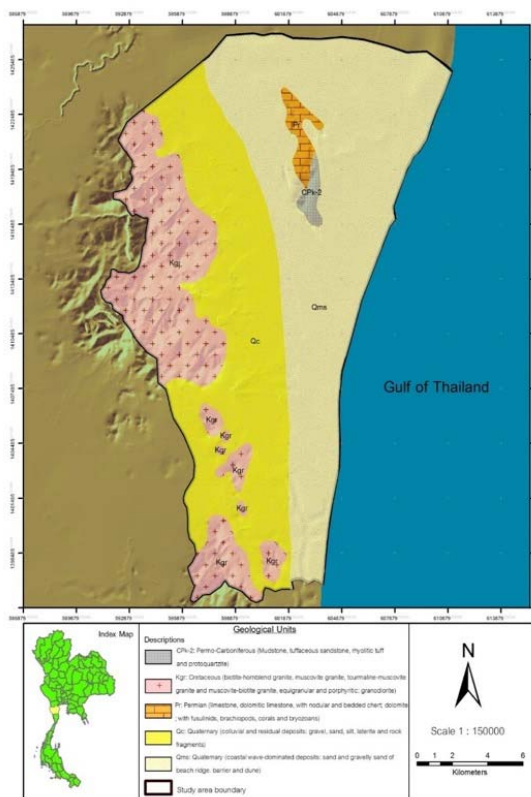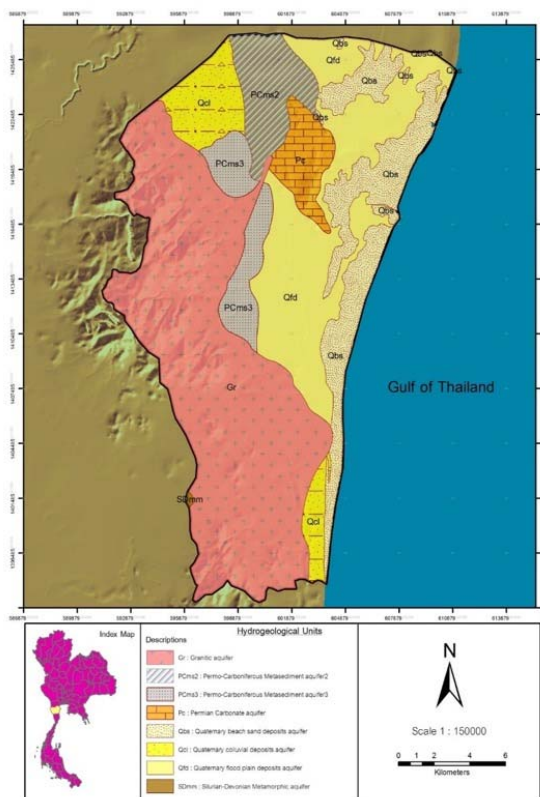
Figure 3.

114
115
116
117
118
119
120
121
122
123

124

125

126

127

Schlumberger Electrode Arrangement
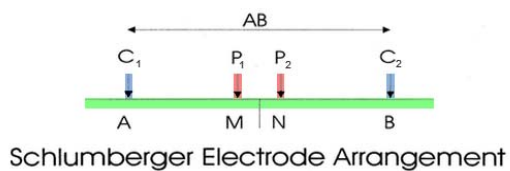
128

129   **Figure 4.**

130

131

132

133

134

135

136

137

138

139

140

141

142

143

144

145

146

147

148

149

150

151

152

153

154

155

156

157

158

159

160

Figure 5.

161
162
163
164
165
166
167
168
169
170
171
172
173
174
175
176
177
178
179
180
181
182
183
184
185
186
187
188
189
190
191
192
193
194
195
196
197
198
199
200
201
202
203
204
205
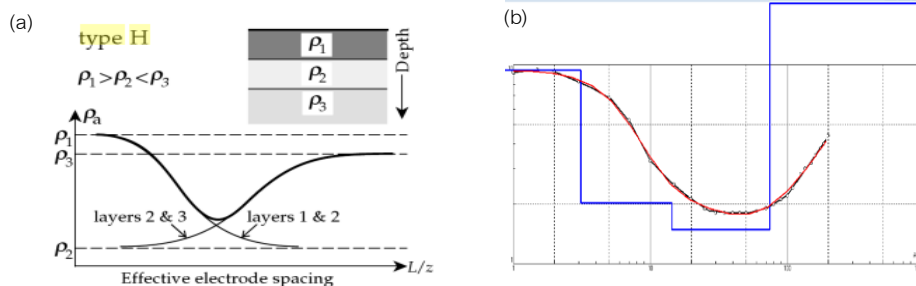
Figure 6.

251
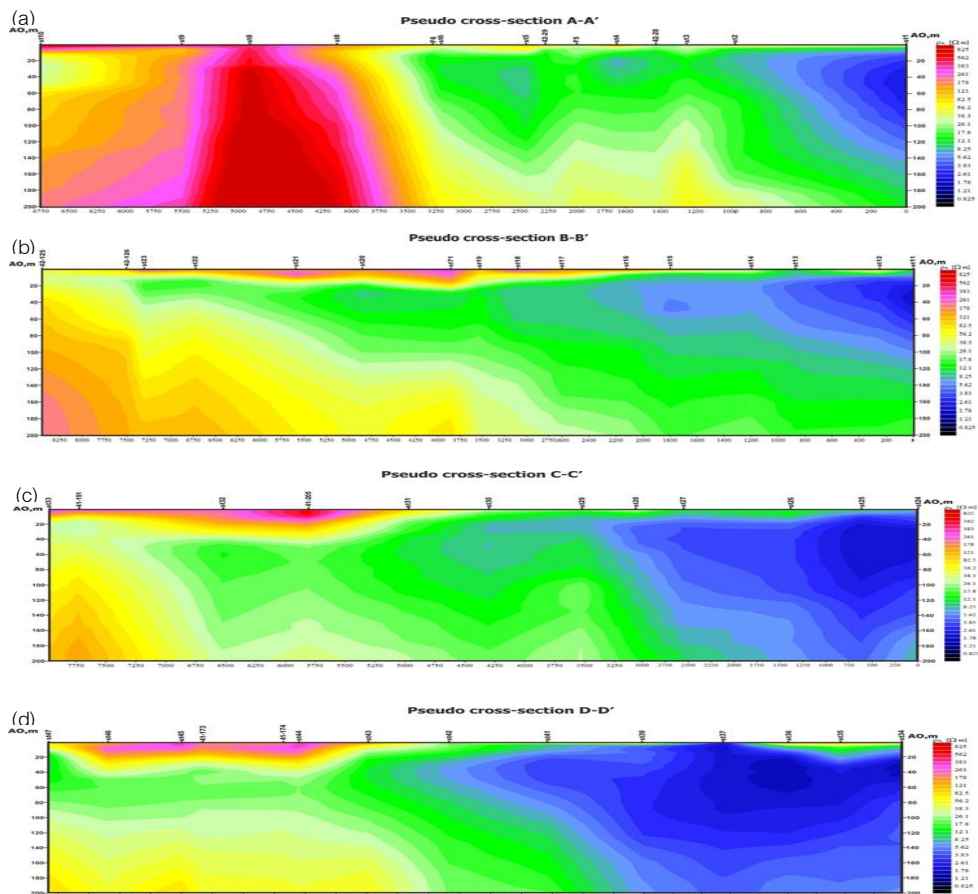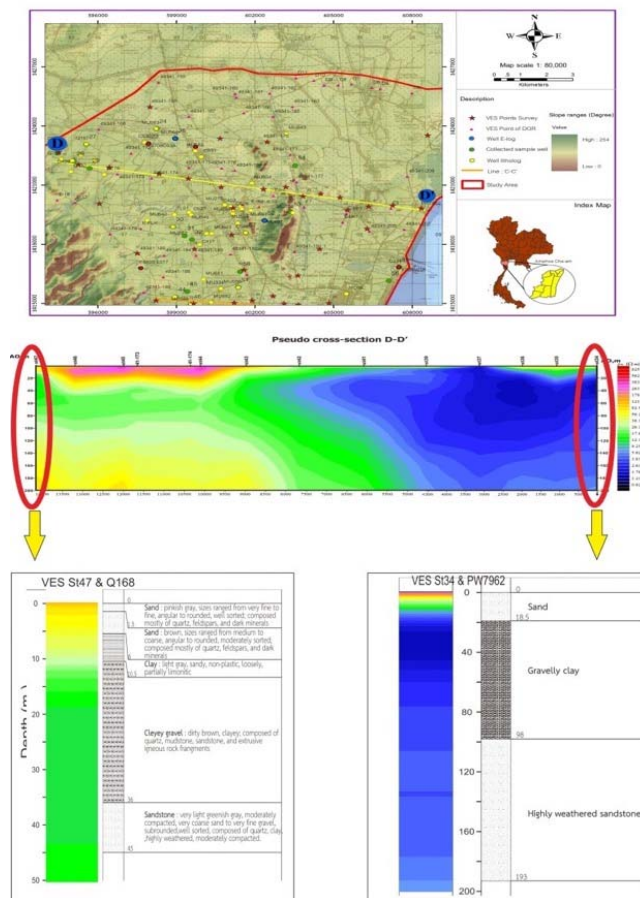
Figure 7.

252
253
254
255
256
257
258
259
260
261
262
263
264
265
266
267
268
269
270
271

272
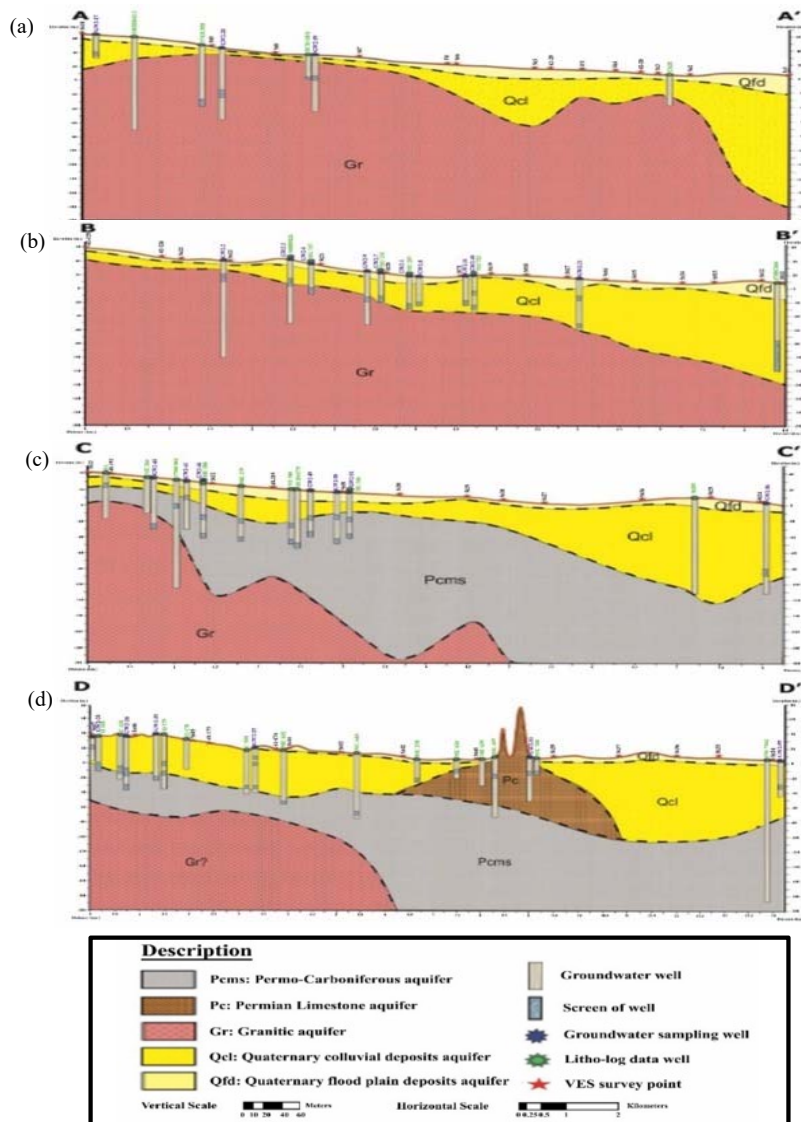
273

274

275

276

277

278

279

280

281

282

283

284

285

286

287

288

289

290

291

292

293

294

Figure 8.

295

296

297

298

299

300
301
302
303
304
305
306
307
308
309
310
311
312
313
314
315
316
317
318
319

Figure 9.

320
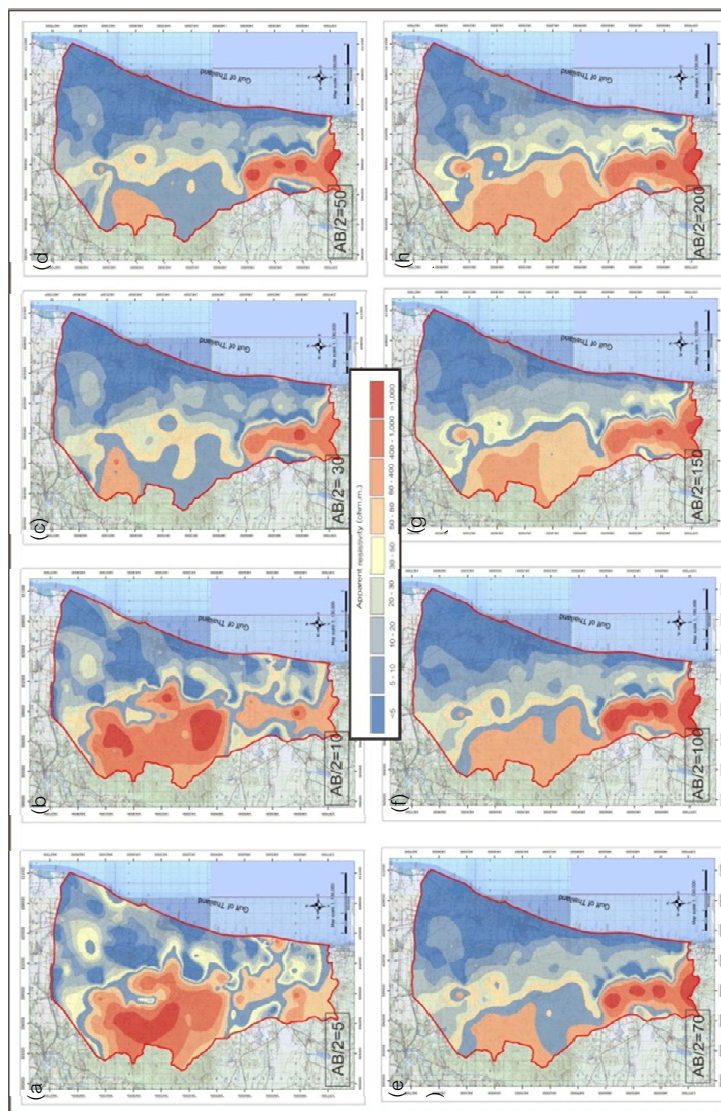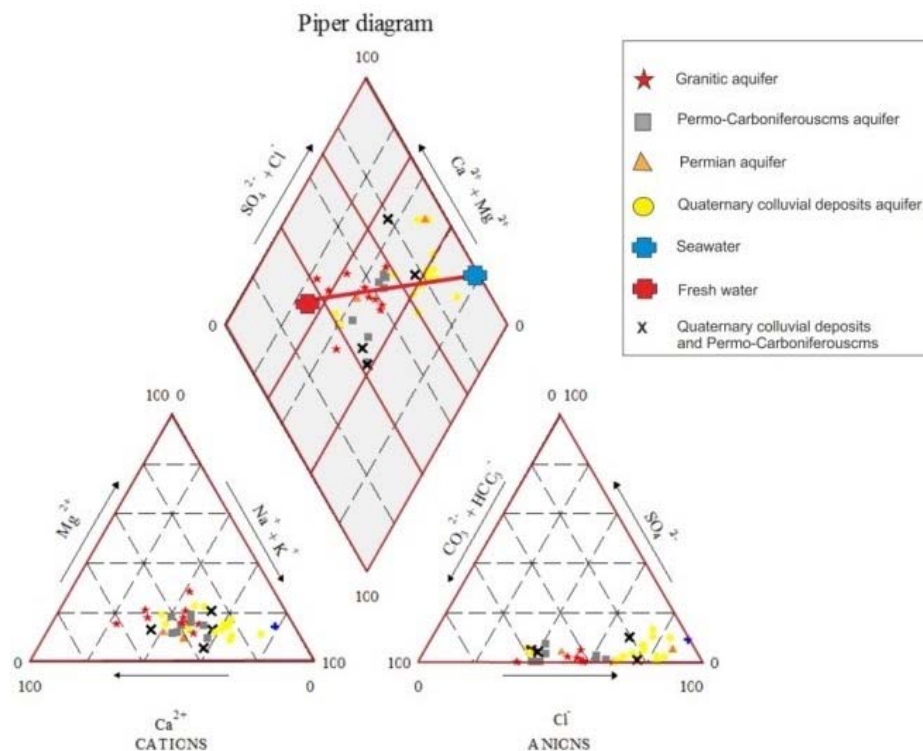
Figure 10.

322
323
324
325
326
327
328
329
330

331
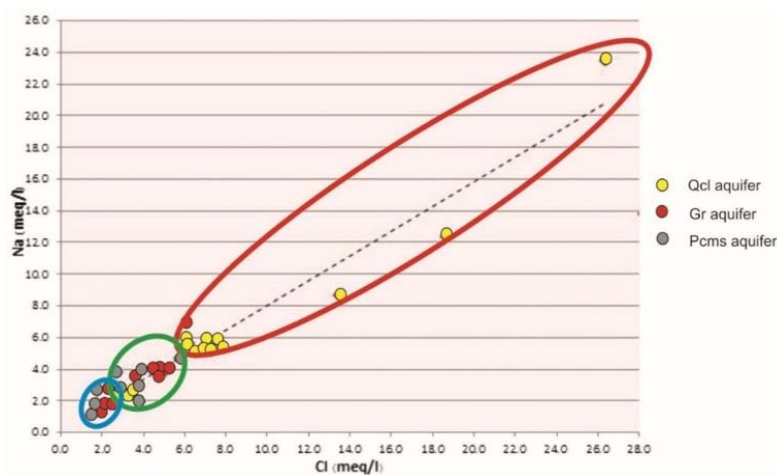
Figure 11.

333
334
335
336
337
338
339
340
341
342
343
344
345
346
347
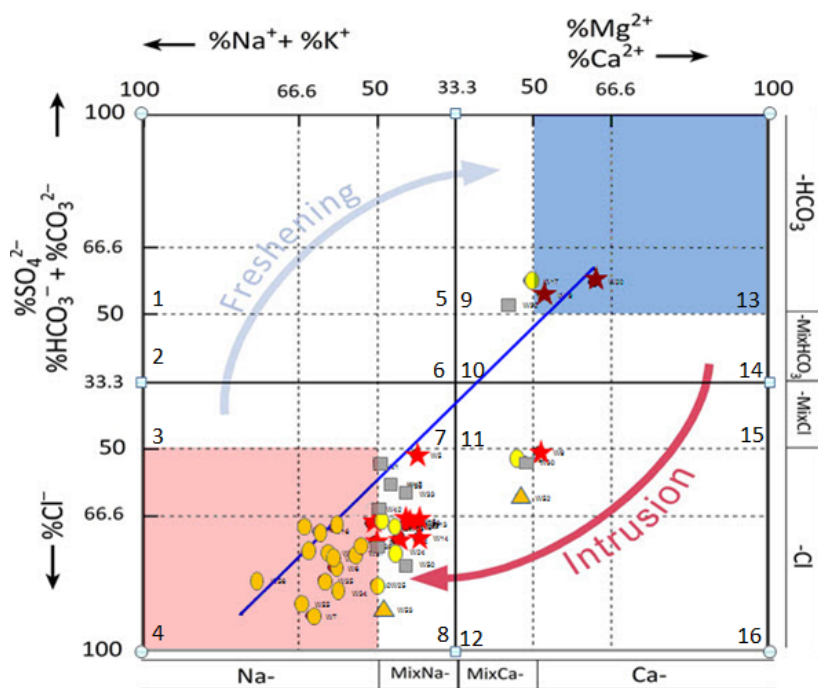
348

349

350   **Figure 12.**

351
352
353
354
355
356
357
358
359
360
361
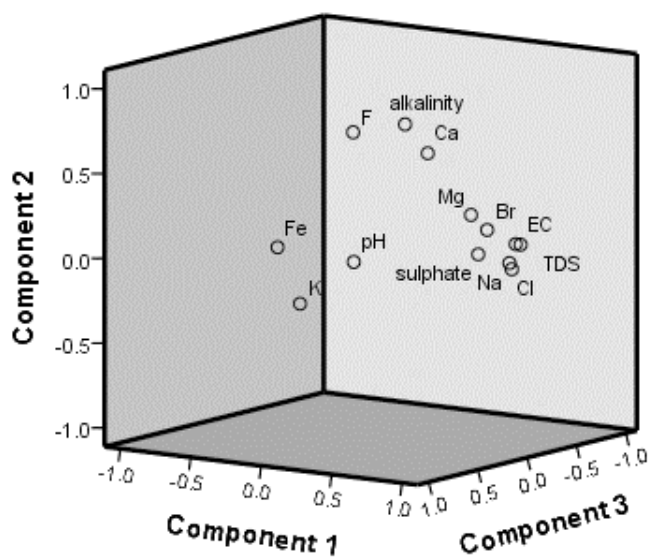362
363
364
365
366
367
368
369
370
371
372
373
374
375
376
377
378
379
380

381
382
383
384
385
386
387
388
389
390

Figure 13.

391

392

393

394

395

396

397

398

399

400

401

402

403

404
405
406
407
408
409
410
411
412
413
414
415
416
417
418
419
420
421
422
423
424
425

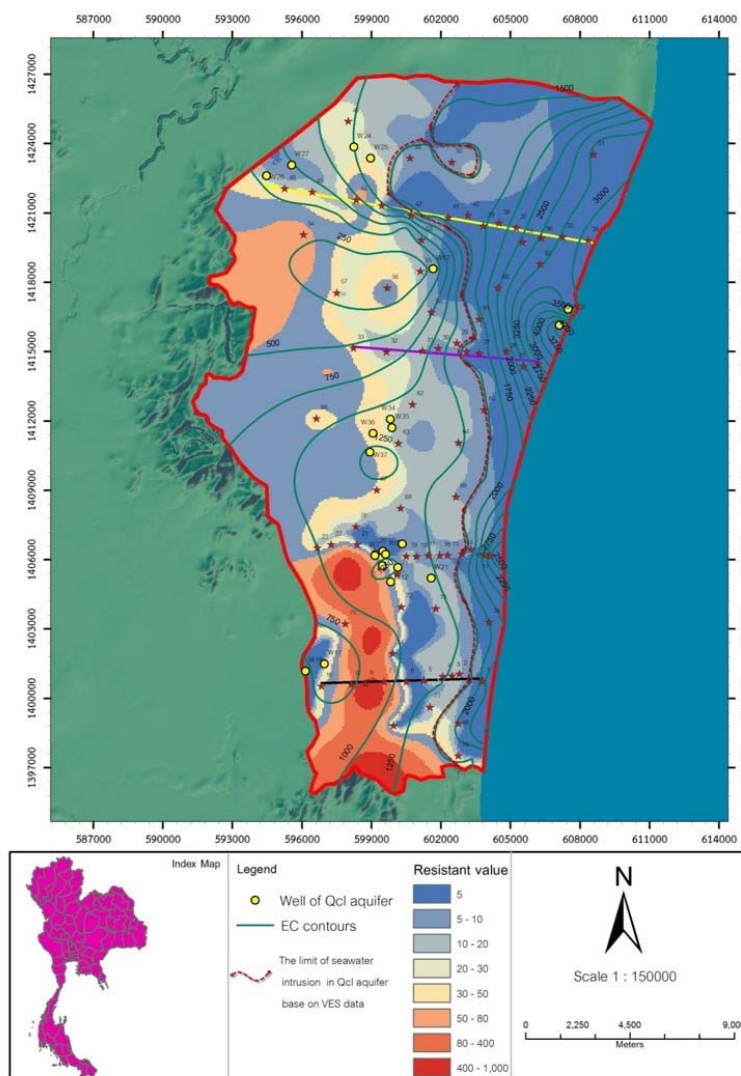**Figure 14.**

426
427